

# Neutrino Cooling of Neutron Stars. Medium effects\*

Dmitri N. Voskresensky

Moscow Institute for Physics and Engineering, Russia, 115409 Moscow,  
Kashirskoe shosse 31; Gesellschaft für Schwerionenforschung GSI, P.O.Box  
110552, D-64220 Darmstadt, Germany

**Abstract.** This review demonstrates that neutrino emission from dense hadronic component in neutron stars is subject of strong modifications due to collective effects in the nuclear matter. With the most important in-medium processes incorporated in the cooling code an overall agreement with available soft  $X$  ray data can be easily achieved. With these findings so called "standard" and "non-standard" cooling scenarios are replaced by one general "nuclear medium cooling scenario" which relates slow and rapid neutron star coolings to the star masses (interior densities). In-medium effects take important part also at early hot stage of neutron star evolution decreasing the neutrino opacity for less massive and increasing for more massive neutron stars. A formalism for calculation of neutrino radiation from nuclear matter is presented that treats on equal footing one-nucleon and multiple-nucleon processes as well as reactions with resonance bosons and condensates. Cooling history of neutron stars with quark cores is also discussed.

## 1 Introduction

The EINSTEIN, EXOSAT and ROSAT observatories have measured surface temperatures of certain neutron stars (NS) and put upper limits on the surface temperatures of some other NS ( cf. [1–3] and further references therein). The data for some supernova remnants indicate rather slow cooling, while the data for several pulsars point to an essentially more rapid cooling.

Physics of NS cooling is based on a number of ingredients, among which the neutrino emissivity of the high density hadronic matter in the star core plays a crucial role. Neutron star temperatures are such that, except first minutes–hours, neutrinos/antineutrinos radiate energy directly from the star without subsequent collisions, since  $\lambda_\nu, \lambda_{\bar{\nu}} \gg R$ , where  $\lambda_\nu, \lambda_{\bar{\nu}}$  are the neutrino and antineutrino mean free paths and  $R$  is star radius. In the so called "standard scenario" of the NS cooling (scenario for slow cooling) the most important channel up to temperatures  $T \sim 10^9$ K belongs to the modified Urca (MU) process  $nn \rightarrow npe\bar{\nu}$ . First estimates of its emissivity were done in [4,5]. References [6,7] recalculated the emissivity of this process in the model, where the nucleon-nucleon (NN) interaction was treated with the help of

---

\* To be published in "Physics of Neutron Star Interiors", Eds. D. Blaschke, N.K. Glendenning, A. Sedrakian, Springer, Heidelberg (2001)

slightly modified free one-pion exchange (FOPE). This important result for the emissivity,  $\varepsilon_\nu[\text{FOPE}]$ , was proved to be by an order of magnitude larger than the previously obtained one. Namely the value  $\varepsilon_\nu[\text{FOPE}]$  was used in various computer simulations resulting in the "standard scenario" of the cooling, e.g. cf. [8–10]. Besides the MU process, in the framework of the "standard scenario" numerical codes included also processes of the nucleon (neutron and proton) bremsstrahlung (NB)  $nn \rightarrow nn\nu\bar{\nu}$  and  $np \rightarrow np\nu\bar{\nu}$ , which lead to a smaller contribution to the emissivity than the MU, cf. [11,6]. Medium effects enter the above two-nucleon (MU and NB) rates mainly through the effective mass of the nucleons which has a smooth density dependence. Therefore within FOPE model the density dependence of the reaction rates is rather weak and the neutrino radiation from a NS depends only very weakly on its mass. This is the reason why the "standard scenario" based on the result [6], though complying well with several slowly cooling pulsars, fails to explain the data of the more rapidly cooling ones. Also "standard scenario" included processes contributing to the emissivity in the NS crust which become important at a lower temperature.

The *non-standard scenario* included so called exotica, associated with different types of direct Urca-like processes, i.e. the pion Urca (PU) [12] and kaon Urca (KU) [13,14]  $\beta$ -decay processes and direct Urca (DU) on nucleons and hyperons [15] possible only in sufficiently dense interiors of rather massive NS. The main difference in the cooling efficiency driven by the DU-like processes on one hand and the MU and NB processes on the other hand lies in the rather different phase spaces associated with these reactions. In the MU and NB case the available phase space is that of a two-fermion origin, while in the pion (kaon)  $\beta$ -decay and DU on nucleons and hyperons it is that of a one-fermion origin. Critical density of pion condensation in NS matter is  $\rho_{c\pi} \simeq (1 \div 3)\rho_0$  depending on the type of condensation (neutral or charged) and the model, see [16–19]. Critical density of kaon condensation is  $\rho_{cK} \simeq (2 \div 6)\rho_0$  depending on the type ( $K^-$  or  $\bar{K}^0$ ,  $S$  or  $P$  wave) and the model, see [20,21]. Critical density for the DU process is  $\rho_{cU} \simeq (2 \div 6)\rho_0$  depending on the model for the equation of state (EQS), see [15,18]. Recent calculations [19] estimated critical density of neutral pion condensation as  $2.5\rho_0$  and for the charged one as  $1.7\rho_0$ , whereas variational calculations [18] argued even for smaller critical densities ( $\simeq 1.3\rho_0$  for  $\pi^0$  condensation). On the other hand the EQS of [18] allows for DU process only at  $\rho > 5\rho_0$ .

There is no bridge between "standard" and "non-standard" scenarios due to complete ignorance of in-medium modifications of  $NN$  interaction which allows for strong polarization of the soft modes (like virtual dressed pion and kaon modes serving a part of in-medium baryon–baryon interaction). *Only due to enhancement of a medium polarization with the baryon density pion condensate may appear and it seems thereby quite inconsistent to ignore the softening effects for  $\rho < \rho_{c\pi}$ , and suddenly switch on the condensate for  $\rho > \rho_{c\pi}$ .*

Now let us basing on the results [22–25,16,26] briefly discuss a general “*nuclear medium cooling scenario*” which treats obvious caveats of two mentioned above scenarios. First of all one observes [22] that in the nuclear matter many new reaction channels are opened up compared to the vacuum processes. Standard Feynman technique fails to calculate in-medium reaction rates if the particle widths are important since there are no free particle asymptotic states in matter. Then summation of all perturbative Feynman diagrams where free Green functions are replaced by the in-medium ones leads to a double counting due to multiple repetitions of some processes (for an extensive discussion of this defect see [27]). This calls a formalism dealing with closed diagrams (integrated over all possible in-medium particle states) with full non-equilibrium Green functions. Such a formalism was elaborated in [23,24] first within quasiparticle approximation (QPA) for nucleons and was called in [24] “*optic theorem formalism (OTF) in non-equilibrium diagram technique*”. It was demonstrated that standard calculation of the rates via squared reaction matrix elements and calculation using OTF coincide within QPA picture for the fermions. In [28] the formalism was generalized to include arbitrary particle widths effects. The latter formalism treats on equal footing one-nucleon and multiple-nucleon processes as well as resonance reaction contributions of the boson origin, as processes with participation of zero sounds and reactions on the boson condensates. Each diagram in the series with full Green functions is free from the infrared divergences. Both, the correct quasiparticle (QP) and quasiclassical limits are recovered.

Except for very early stage of NS evolution (minutes - hours) typical averaged lepton energy ( $\gtrsim T$ ) is larger than the nucleon particle width  $\Gamma_N \sim T^2/\varepsilon_{FN}$  and the nucleons can be treated within the QPA. This observation much simplifies consideration since one can use an intuitive way of separation of the processes according to the available phase space. The one-nucleon processes have the largest emissivity (if they are not forbidden by energy-momentum conservations), then two-nucleon processes come into play, etc.

In the temperature interval  $T_c < T < T_{opac}$  ( $T_c$  is typical temperature for the nucleon pairing and  $T_{opac}$  is typical temperature at which neutrino/antineutrino mean free path  $\lambda_\nu/\lambda_{\bar{\nu}}$  is approximately equal to the star radius  $R$ ) the neutrino emission is dominated by the medium modified Urca (MMU) and medium nucleon bremsstrahlung (MNB) processes if one-nucleon reactions like DU, PU and KU are forbidden, as it is the case for  $\varrho < \varrho_{cU}, \varrho_{c\pi}, \varrho_{cK}$ . Corresponding diagrams for MMU process are schematically shown in Fig. 1. References [22–25,16] considered  $NN$  interaction within Fermi liquid Landau–Migdal approach. They incorporated the softening of the medium one-pion exchange (MOPE) mode, other medium polarization effects, like nucleon-nucleon correlations in the vertices, renormalization of the local part of  $NN$  interaction by the loops, as well as the possibility of the neutrino emission from the intermediate reaction states and resonance DU-like reactions going on zero sounds and the boson condensates. References

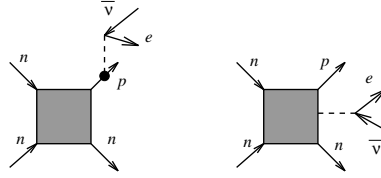


**Fig. 1.** Antineutrino emission from a nucleon leg (left graph) and from intermediate scattering states (right) in MMU process. Full dot includes weak coupling vertex renormalization.

[23,25,16] have demonstrated that for  $\varrho \gtrsim \varrho_0$  second diagram of Fig. 1 gives the main contribution to the emissivity of MMU process rather than the first one which contribution has been earlier evaluated in the framework of FOPE model in [6]. This fact essentially modifies the absolute value as well as the density dependence of the  $nn \rightarrow npe\bar{\nu}$  process rate which becomes to be very sharp. Thereby, for stars of masses larger than the solar mass the resulting emissivities were proved to be substantially larger than those values calculated in FOPE model. With increase of the star mass (central density) pion mode continues to soften and MMU and MNB rates still increase. At  $\varrho > \varrho_{c\pi}$  pion condensation begins to contribute. Actually, the condensate droplets may be exist already at a smaller density if the mixed phase is appeared, as suggested in [29]. At  $T > T_{melt}$ , where  $T_{melt}$  is the melting temperature, roughly  $\sim$  several MeV, the mixed phase is in liquid state and PU processes on independent condensate droplets are possible. At  $T < T_{melt}$  condensate droplets are placed in a crystalline lattice that substantially suppresses corresponding neutrino processes.

Reference [12] considered the reaction channel  $n \rightarrow p\pi_c^- e\bar{\nu}$ , whereas [22,23] included other possible pion  $\pi^+$ ,  $\pi^\pm$ ,  $\pi^0$  condensate processes with charged and neutral currents (e.g., like  $n\pi_c^0 \rightarrow pe\bar{\nu}$ ,  $n\pi_c^+ \rightarrow p\nu\bar{\nu}$  and  $n\pi_c^0 \rightarrow n\nu\bar{\nu}$ ) as well as resonance reactions going on zero sounds which are also possible at  $\varrho < \varrho_{c\pi}$ . Due to  $NN$  correlations all pion condensate rates are significantly suppressed (by factors  $\sim 10 - 100$  compared to first estimate [12], see [30,22,23,31]. At  $\varrho \sim \varrho_{c\pi}$  both MMU and PU processes are of the same order of magnitude [23] demonstrating a smooth transition to higher densities (star masses) being absent in the "standard" and "non-standard" scenarios.

For  $T < T_c$  the reactions of neutrino pair radiation from superfluid nucleon pair breaking and formation (NPBF) shown in Fig. 2 become to be dominant processes. The neutron pair breaking and formation (nPBF) process for the case of the  $1S_0$  pairing was first calculated in [32] using standard Bogolyubov technique. Later this process was independently calculated in [24,25] as demonstration of efficiency of OTF within the closed non-equilibrium diagram technique developed there. Moreover [24] calculated emissivity of the corresponding process on proton (pPFB) taking into account strong coupling  $p\nu\bar{\nu}$  vertex renormalization (see first diagram (19) below). It

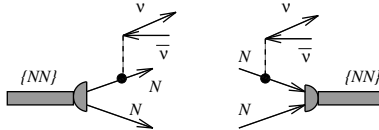


**Fig. 2.** Neutrino–antineutrino emission from Cooper pair-breaking (left graph) and pair-formation processes (right graph).

results in one-two order of magnitude enhancement of pPFB emissivity (for  $\varrho \sim (1.5 \div 3)\rho_0$ ) compared to that would be estimated with the vacuum vertex, leading to that both nPFB and pPFB emissivities can be of the same order of magnitude. Emissivities of NPBF processes have the same suppression factor  $\sim \exp(-2\Delta/T)$  as MU, NB, MMU and MNB at  $T < T_c$  but compared to the latter the NPBF processes have a large one nucleon phase space volume. Ref. [24] and then [16] also sketched how to incorporate  $3P_2$  pairing (the developed formalism easily allows to do it) indicating that exponential suppression of the specific heat and the emissivity is to be replaced by only a power law suppression when the gap vanishes at the Fermi sphere poles. This is precisely the case for the  $3P_2(|m_J|=2)$  pairing, where  $m_J$  is projection of the total pair momentum onto quantization axis. This idea was then worked out in [33–35], without reference.

I would also like to do a historic remark relating to estimation of the NPBF processes since in some works (e.g., see [36,35]) was expressed a surprise why these processes were not on a market during many years. First work [32], although found correct analytic expression for  $1S_0$  pairing of neutrons, numerically underestimated the emissivity by an order of magnitude. Also there was no statement on the dominance of the process in the cooling scenario (i.e. over the MU). Asymptotic behaviour of the emissivity  $\varepsilon[\text{nPBF}] \sim 10^{20} T_9^7 \exp(-2\Delta/T)$  for  $T \ll \Delta$ ,  $T_9 = T/10^9 \text{K}$ , as follows from expression (1b) of [32] and from their rough asymptotic estimate of the integral (see below (13b)), shows up nor a large one nucleon phase space factor ( $\sim 10^{28}$ ) nor appropriate temperature behaviour. Namely this underestimation of the rate in [32] (we again point out that analytic expression (1a) is correct) and absence of mentioning of possible dominance of the process over MU, became the reason that this important result was overlooked during many years. Reference [24] overlooked sign of anomalous diagram for  $S$  pairing and included  $\propto g_A^2$  term ( $g_A$  is axial-vector coupling constant) which should be absent for  $S$  pairing giving, nevertheless, the main contribution for the  $3P_2$  pairing case. A reasonable numerical estimate of the emissivity was presented valid for both  $S$  and  $P$  pairings (except  $|m_J|=2$  case) including  $NN$  correlation effects into consideration. Uncertainty of this estimate is given by a factor  $(0.5 \div 2)$  which is allowed by variation of not too well known correlation factors. Namely this estimate was then incorporated within the cooling code in [26]. Correct asymptotic behaviour of the emissivity is  $\varepsilon[\text{nPFB, pPFB}] \sim 10^{28} (\Delta/\text{MeV})^7 (T/\Delta)^{1/2} \exp(-2\Delta/T)$  for  $T \ll \Delta$ ,

that showed up a huge one-nucleon phase space factor and very moderate  $T$  dependence of the pre-factor. Thereby the value of the rate was related in [24] to the value of the pairing gap. The possibility of the dominant role of this process (even compared to enhanced MMU and PU rather than only to MU) was unambiguously stressed. Unfortunately [24] had a number of obvious misprints which were partially corrected in subsequent papers. Although it does not excuse the authors these misprints can be easily treated by an *attentive* reader. Importance of NPFB processes was then once more stressed in review [16]. Reference [26] was the first that quoted the previous result [32]. It incorporated most important in-medium effects in the cooling code, among them nPBF and pPBF as equally important processes. The latter process was then rediscovered in [34] as negligible one due to ignorance there of correlations in weak interaction vertices. Work [36] supported conclusion of [26] on importance of NPBF processes as governing the cooling scenario at  $T < T_c$ .

The medium modifications of all the above mentioned rates result in a pronounced density dependence (for NPBF processes mainly via dependence of the pairing gaps on the density and dependence on the  $NN$  correlation factors), which links the cooling behavior of a neutron star decisively to its mass [22,23,16,26]. As the result, the above mentioned medium modifications lead to a more rapid cooling than obtained in the *"standard scenario"*. Hence they provide a possible explanation for the observed deviations of some of the pulsar temperatures from the *"standard"* cooling. Particularly, they provide a smooth transition from *"standard"* to *"non-standard"* cooling for increasing central star densities, i.e., star masses. Thus by means of taking into account of most important in-medium effects in the reaction rates one is indeed able to achieve an appropriate agreement with both the high as well as the low observed pulsar temperatures that leads to the new *"nuclear medium cooling scenario"*. Using a collection of modern EQS for nuclear matter, which covered both relativistic as well as non-relativistic models, [26] also has demonstrated a relative robustness of these in-medium cooling mechanisms against variations in the EQS of dense NS matter (for EQS that allow for a wide dense hadronic region in NS).

At initial stage ( $T > T_{opac}$ ) the newly formed hot NS is opaque for neutrinos/antineutrinos. Within FOPE model the value  $T_{opac}$  was estimated in [6]. Elastic scatterings were included in [37,38] and pion condensation effect on the opacity was discussed in [39]. Medium effects dramatically affect the neutrino/antineutrino mean free paths, since  $\lambda_{\nu(\bar{\nu})} \propto 1/|M|^2$ , where  $M$  is the reaction matrix element. Thereby, one-nucleon elastic scattering processes, like  $N\nu \rightarrow N\nu$ , for energy and momentum transfer  $\omega < qv_{FN}$  are suppressed by  $NN$  correlations [24,16,40,41]. Neutrino/antineutrino absorption in two-nucleon MMU and MNB processes is substantially increased with the density (since  $|M|^2$  for MMU and MNB processes increases with the density) [23,24,16]. Thus more massive NS are opaque for neutrinos up to

lower temperatures that also results in a delay of neutrino pulse. Within the QPA for the nucleons the value  $T_{opac}$  was estimated with taking into account of medium effects in [23,16]. References [42,43,16] considered possible consequences of such a delay for supernova explosions. On the other hand, at  $T > (1 \div 2)\text{MeV}$  one should take care of the neutrino/antineutrino radiation in multiple  $NN$  scatterings (Landau–Pomeranchuk–Migdal (LPM) effect) when averaged neutrino–antineutrino energy,  $\omega_{\nu\bar{\nu}} \sim \text{several } T$ , becomes to be smaller than the nucleon width  $\Gamma_N$  [28]. Numerical evaluations of  $\Gamma_N$  in application to MNB processes were done in [44] and [45] within the Brückner scheme and the Bethe–Salpeter equation, respectively. The LPM effect suppresses the rates of the neutrino elastic scattering processes on nucleons and also it suppresses MNB rates. For NS of rather low mass ( $\lesssim M_\odot$ ) the suppression of the rates of neutral current processes due to the multiple collision coherence effect prevails over the enhancement due to the pion softening, and for sufficiently massive NS ( $\gtrsim 1.4M_\odot$ ) the enhancement prevails the suppression. MMU emissivity remains to be almost unaffected by the LPM effect since averaged  $\bar{\nu}e$  energy  $\sim p_{F_e}$  is rather large ( $\gg \Gamma_N$ ).

Besides pion and kaon condensates, under current discussion is the possibility of the presence of the quark matter at sufficiently high baryon densities. Thereby, these phases may exist in most massive NS. Also a particular discussion is devoted to the possibility of the existence of less massive, stable or metastable, dense nuclei-stars glued by the condensates or by strange quarks, cf. [46,47,16,48,49]. Uncertainty in these predictions relate to the poorly known EQS at high baryon densities. Several possible types of stars differing in their values of the bag constant  $B$  were discussed: ordinary NS without any quark core, hybrid neutron stars (HNS) with quark matter present only in their deep interiors (for somewhat intermediate values of  $B$ ), NS with large quark core (QCNS), a narrow hadron layer and a crust typical for a NS, and quark stars (QS) with a tiny crust of normal matter and with no crust (both for low  $B$ ). If these objects are produced in supernova explosions within ordinary mechanism of blowing off the mantle, they are rather massive HNS. If an extra support for the blowing off the matter arises, there may appear less massive objects like QCNS, QS and may be even objects of arbitrary size.

Especial interest for the discussion of cooling of HNS, QCNS, and QS is motivated by recent works [50,51] which demonstrated possibility of diquark condensates characterized by large pairing gaps ( $\Delta_q \lesssim 100 \text{ MeV}$ ) in dense quark matter. The two-flavor (2SC) and the three-flavor (3SC) color superconducting phases allow for unpaired quarks of one color whereas in the color-flavor locking (CFL) phase all the quarks are paired. Presence of large quark gap may significantly affect the cooling history of HS, QCNS and QS. Thus it is interesting to confront this possibility to the observational data. Cooling of QCNS, and QS was discussed in [52,53] and the case of HNS was considered in [54,53]. In difference with [52,54] more recent work [53]

incorporated the heat transport being important during a longer period of time compared to that can be in absence of the color superconducting quark matter.

The paper is organized as follows. Sect. 2 discusses basic ideas of the Fermi liquid approach to description of nuclear matter. The  $NN$  interaction amplitude is constructed with an explicit treatment of long-ranged soft pion mode and vertex renormalizations due to  $NN$  correlations. The meaning of the pion softening effect is clarified and a comparison of MOPE and FOPE models is given. Also renormalization of the weak interaction in NS matter is performed. Sect. 3 discusses the cooling of NS at  $T < T_{opac}$ . Comparison of emissivities of MMU and MU processes shows a significant enhancement of in-medium rates. Then we discuss DU-like processes and demonstrate medium effect due to vertex renormalizations. The role of in-medium mechanisms in the cooling evolution of NS is then demonstrated within a realistic cooling code. Next we consider influence of in-medium effects on the neutrino mean free path at initial stage of NS cooling. Essential role of multiple  $NN$  collisions is discussed. Sect. 4 presents OTF in non-equilibrium closed diagram technique in the framework of QPA for the nucleons and also beyond the QPA incorporating genuine particle width effects. In the last Sect. 5 following [53] we review recent results on the cooling of HNS.

## 2 Nuclear Fermi liquid description

### 2.1 $NN$ interaction. Separation of hard and soft modes

At temperatures of our interest ( $T \ll \varepsilon_{Fn}$ ) neutrons are only slightly excited above their Fermi sea and all the processes occur in a narrow vicinity of  $\varepsilon_{Fn}$ . In such a situation Fermi liquid approach seems to be the most efficient one. Within this approach the long-ranged diagrams are treated explicitly whereas short-scale diagrams are supposed to be the local quantities given by phenomenological so called Landau-Migdal (LM) parameters. Thus using argumentation of Fermi liquid theory [55–57,16] the retarded  $NN$  interaction amplitude is presented as follows (see also [58])

$$\text{[Solid Square]} = \text{[Hatched Circle]} + \text{[Hatched Circle + Loop]} + \text{[Hatched Circle + Double-Line Loop]} \quad (1)$$

where

$$\text{[Hatched Circle]} = \text{[Hatched Circle]} + \text{[Double-Wavy Line]} \quad (2)$$

The solid line presents the nucleon, whereas double-line, the  $\Delta$  isobar. The double-wavy line corresponds to the exchange of the free pion with inclusion



of the contributions of the residual  $S$  wave  $\pi NN$  interaction and  $\pi\pi$  scattering, i.e. the residual irreducible interaction to the nucleon particle-holes and delta-nucleon holes. The full particle-hole, delta-nucleon hole and pion irreducible block (first block in (2)) is by its construction essentially more local than contributions given by explicitly presented graphs. Thereby, it is parameterized with the help of the LM parameters. In the standard Landau Fermi liquid theory fermions are supposed to be at their Fermi surface and the Landau parameters are further expanded in Legendre polynomials in the angle between fermionic momenta. Luckily, only zero and first harmonics enter physical quantities. The momentum dependence of the residual part of nuclear forces is expected to be not as pronounced and one can avoid this expansion. Then these parameters, i.e.  $f_{nn}$ ,  $f_{np}$  and  $g_{nn}$ ,  $g_{np}$  in scalar and spin channels respectively, are considered as slightly momentum dependent quantities. In principle, they should be calculated as functions of the density, neutron and proton concentrations, energy and momentum but, simplifying, one can extract them from analysis of experimental data.

The part of interaction involving  $\Delta$  isobar is analogously constructed

$$\text{Shaded circle with 4 arrows} = \text{Cross-hatched circle with 4 arrows} + \text{Wavy line with 4 arrows} \quad (3)$$

The main part of the  $N\Delta$  interaction is due to the pion exchange. Although information on local part of the  $N\Delta$  interaction is rather scarce, one can conclude [16,19] that the corresponding LM parameters are essentially smaller than those for  $NN$  interaction. Besides, at small transferred energies  $\omega \ll m_\pi$  the  $\Delta$ -nucleon hole contribution is a smooth function of  $\omega$  and  $k$  in difference with the nucleon-nucleon hole ( $NN^{-1}$ ) contribution. Therefore and also for simplicity we neglect the first graph in r.h.s. of (3).

Straightforward resummation of (1) in neutral channel yields [24,16]

$$\Gamma_{\alpha\beta}^R = \begin{array}{c} \alpha \\ \swarrow \quad \searrow \\ \blacksquare \\ \swarrow \quad \searrow \\ \beta \end{array} = C_0 (\mathcal{F}_{\alpha\beta}^R + \mathcal{Z}_{\alpha\beta}^R \boldsymbol{\sigma}_1 \cdot \boldsymbol{\sigma}_2) + f_{\pi N}^2 \mathcal{T}_{\alpha\beta}^R (\boldsymbol{\sigma}_1 \cdot \mathbf{k})(\boldsymbol{\sigma}_2 \cdot \mathbf{k}), \quad (4)$$

$$\begin{aligned} \mathcal{F}_{\alpha\beta}^R &= f_{\alpha\beta} \gamma(f_{\alpha\beta}), \quad \mathcal{Z}_{nn}^R = g_{nn} \gamma(g_{nn}), \quad \mathcal{Z}_{np}^R = g_{np} \gamma(g_{nn}), \quad \alpha, \beta = (n, p), \\ \mathcal{T}_{nn}^R &= \gamma^2(g_{nn}) D_{\pi^0}^R, \quad \mathcal{T}_{np}^R = -\gamma_{pp} \gamma(g_{nn}) D_{\pi^0}^R, \quad \mathcal{T}_{pp}^R = \gamma_{pp}^2 D_{\pi^0}^R, \\ \gamma^{-1}(x) &= 1 - 2xC_0 A_{nn}^R, \quad \gamma_{pp} = (1 - 4gC_0 A_{nn}^R) \gamma(g_{nn}), \end{aligned} \quad (5)$$

$f_{nn} = f_{pp} = f + f'$ ,  $f_{np} = f - f'$ ,  $g_{nn} = g_{pp} = g + g'$ , and  $g_{np} = g - g'$ , dimensional normalization factor is usually taken to be  $C_0 = \pi^2/[m_N p_F(\varrho_0)] \simeq 300 \text{ MeV} \cdot \text{fm}^3 \simeq 0.77 m_\pi^{-2}$ ,  $D_{\pi^0}^R$  is the full retarded Green function of  $\pi^0$ ,  $A_{\alpha\beta}$  is the corresponding  $NN^{-1}$  loop (without spin degeneracy factor 2)

$$A_{\alpha\beta} = \begin{array}{c} \beta \\ \circlearrowleft \\ \alpha^{-1} \end{array}, A_{nn}(\omega \simeq q) \simeq m_n^{*2}(4\pi^2)^{-1} \left( \ln \frac{1+v_{Fn}}{1-v_{Fn}} - 2v_{Fn} \right), \quad (6)$$

$A_{nn} \simeq -m_n^* p_{Fn} (2\pi^2)^{-1}$ , for  $\omega \ll q v_{Fn}, q \ll 2p_{Fn}$ , and we for simplicity neglect proton hole contributions due to a small concentration of protons. Resummation of (1) in the charged channel yields

$$\tilde{\Gamma}_{np}^R = \begin{array}{c} n \\ \swarrow \quad \searrow \\ \blacksquare \\ \swarrow \quad \searrow \\ p \quad p \end{array} = C_0 \left( \tilde{\mathcal{F}}_{np}^R + \tilde{\mathcal{Z}}_{np}^R \boldsymbol{\sigma}_1 \cdot \boldsymbol{\sigma}_2 \right) + f_{\pi N}^2 \tilde{\mathcal{T}}_{np}^R (\boldsymbol{\sigma}_1 \cdot \mathbf{k})(\boldsymbol{\sigma}_2 \cdot \mathbf{k}), \quad (7)$$

$$\begin{aligned} \tilde{\mathcal{F}}_{np}^R &= 2f' \tilde{\gamma}(f'), \quad \tilde{\mathcal{Z}}_{np}^R = 2g' \tilde{\gamma}(g'), \quad \tilde{\mathcal{T}}_{np}^R = \tilde{\gamma}^2(g') D_{\pi^-}^R, \\ \tilde{\gamma}^{-1}(x) &= 1 - 4xC_0 A_{np}^R. \end{aligned} \quad (8)$$

The LM parameters are rather unknown for isospin asymmetric nuclear matter and for  $\varrho > \varrho_0$ . Although some evaluations of these quantities have been done, much work is still needed to get convincing results. Therefore for estimates we will use the values extracted from atomic nucleus experiments. Using argumentation of a relative locality of these quantities we will suppose the LM parameters to be independent on the density for  $\varrho > \varrho_0$ . One then can expect that the most uncertain will be the value of the scalar constant  $f$  due to essential role of the medium-heavy  $\sigma$  meson in this channel. But this parameter does not enter the tensor force channel being most important in our case. Unfortunately, there are also essential uncertainties in numerical values of some of the LM parameters even for atomic nuclei. These uncertainties are, mainly, due to attempts to get the best fit of experimental data in each concrete case slightly modifying parameterization used for the residual part of the  $NN$  interaction. E.g., calculations [56] gave  $f \simeq 0.25$ ,  $f' \simeq 1$ ,  $g \simeq 0.5$ ,  $g' \simeq 1$  whereas [59–61], including QP renormalization pre-factors, derived the values  $f \simeq 0$ ,  $f' \simeq 0.5 \div 0.6$ ,  $g \simeq 0.05 \pm 0.1$ ,  $g' \simeq 1.1 \pm 0.1$ .

Typical energies and momenta entering  $NN$  interaction of our interest are  $\omega \simeq 0$  and  $k \simeq p_{Fn}$ . Then rough estimation yields  $\gamma(g_{nn}, \omega \simeq 0, k \simeq p_{Fn}, \varrho = \varrho_0) \simeq 0.35 \div 0.45$ . For  $\omega = k \simeq T$  typical for the weak processes with participation of  $\nu\bar{\nu}$  one has  $\gamma^{-1}(g_{nn}, \omega \simeq k \simeq T, \varrho = \varrho_0) \simeq 0.8 \div 0.9$ .

## 2.2 Virtual Pion Mode

Resummation of diagrams yields the following Dyson equation for pions

$$\begin{array}{c} \text{wavy line} \\ \text{---} \end{array} = \begin{array}{c} \text{wavy line} \\ \text{---} \end{array} + \begin{array}{c} \text{wavy line} \\ \text{---} \end{array} \begin{array}{c} \text{loop with pion} \end{array} + \begin{array}{c} \text{wavy line} \\ \text{---} \end{array} \begin{array}{c} \text{loop with pion and nucleon} \end{array} + \begin{array}{c} \text{wavy line} \\ \text{---} \end{array} \boxed{\Pi_{\text{res}}^R} \begin{array}{c} \text{wavy line} \\ \text{---} \end{array} \quad (9)$$

The  $\pi N \Delta$  full-dot-vertex includes a background correction due to the presence of the higher resonances,  $\Pi_{res}^R$  is the residual retarded pion self-energy that includes the contribution of all the diagrams which are not presented explicitly in (9), as  $S$  wave  $\pi NN$  and  $\pi\pi$  scatterings (included by double-wavy line in (2)). The full vertex takes into account  $NN$  correlations

$\text{Diagram 1} = \text{Diagram 2} + \text{Diagram 3} \quad (10)$

Due to that the nucleon particle-hole part of  $\Pi_{\pi^0}$  is  $\propto \gamma(g_{nn})$  and the nucleon particle-hole part of  $\Pi_{\pi^\pm}$  is  $\propto \gamma(g')$ . The value of the  $NN$  interaction in the pion channel is determined by the full pion propagator at small  $\omega$  and  $k \simeq p_{Fn}$ , i.e. by the quantity  $\tilde{\omega}^2(k) = -(D_\pi^R)^{-1}(\omega = 0, k, \mu_\pi)$ . Typical momenta of our interest are  $k \simeq p_{Fn}$ . Indeed the momenta entering the  $NN$  interaction in MU and MMU processes are  $k = p_{Fn}$ , the momenta governing the MNB are  $k = k_0$  [23] where the value  $k = k_0 \simeq (0.9 \div 1)p_{Fn}$  corresponds to the minimum of  $\tilde{\omega}^2(k)$ . The quantity  $\tilde{\omega} \equiv \tilde{\omega}(k_0)$  has the meaning of the *effective pion gap*. It is different for  $\pi^0$  and for  $\pi^\pm$  since neutral and charged channels are characterized by different diagrams permitted by charge conservation, thus also depending on the value of the pion chemical potential,  $\mu_{\pi^+} \neq \mu_{\pi^-} \neq 0$ ,  $\mu_{\pi^0} = 0$ . For  $T \ll \varepsilon_{Fn}, \varepsilon_{Fp}$ , one has  $\mu_{\pi^-} = \mu_e = \varepsilon_{Fn} - \varepsilon_{Fp}$ , as follows from equilibrium conditions for the reactions  $n \rightarrow p\pi^-$  and  $n \rightarrow pe\bar{\nu}$ .

Change of the sign of  $\tilde{\omega}^2$  symbolizes the pion condensate phase transition. Typical density behaviour of  $\tilde{\omega}^2$  is shown in Fig. 3. At  $\varrho < (0.5 \div 0.7)\varrho_0$ , one

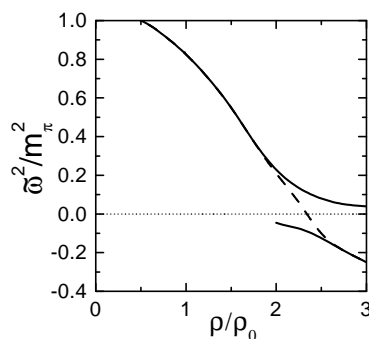


**Fig. 3.** Effective pion gap (for  $\mu_{\pi^0} = 0$ ) versus baryon density, see [16].

has  $\tilde{\omega}^2 = m_\pi^2 - \mu_\pi^2$ . For such densities the value  $\tilde{\omega}^2(p_{Fn})$  essentially deviates from  $m_\pi^2 - \mu_\pi^2$  tending to  $m_\pi^2 + p_{Fn}^2 - \mu_\pi^2$  in small density limit.

At the critical point of the pion condensation ( $\varrho = \varrho_{c\pi}$ ) the value  $\tilde{\omega}^2$  with artificially switched off  $\pi\pi$  fluctuations (dashed line in Fig. 3) changes its sign. In reality  $\pi\pi$  fluctuations are significant in the vicinity of the critical point

and there occurs the first-order phase transition to the inhomogeneous pion-condensate state [62–64]. Thereby there are two branches (solid curves in Fig. 3) with positive and respectively negative values for  $\tilde{\omega}^2$ . Calculations of [64] demonstrated that at  $\varrho > \varrho_{c\pi}$  the free energy of the state with  $\tilde{\omega}^2 > 0$ , where the pion mean field is zero, becomes larger than that of the corresponding state with  $\tilde{\omega}^2 < 0$  and a finite mean field. Therefore at  $\varrho > \varrho_{c\pi}$  the state with  $\tilde{\omega}^2 > 0$  is metastable and the state with  $\tilde{\omega}^2 < 0$  and the pion mean field  $\varphi_\pi \neq 0$  becomes the ground state.

The quantity  $\tilde{\omega}^2$  demonstrates how much the virtual (particle-hole) mode with pion quantum numbers is softened at given density. The ratio  $\alpha = D_\pi[\text{med.}]/D_\pi[\text{vac.}] \simeq 6$  for  $\varrho = \varrho_0$ ,  $\omega = 0$ ,  $k = p_{FN}$  and for isospin symmetric nuclear matter. However this essential so called "pion softening" [57] does not significantly enhance the  $NN$  scattering cross section due to a simultaneous essential suppression of the  $\pi NN$  vertex by  $NN$  correlations. Indeed, the ratio of the  $NN$  cross sections calculated with FOPE and MOPE is

$$R = \frac{\sigma[\text{MOPE}]}{\sigma[\text{FOPE}]} \simeq \frac{\gamma^4(g', \omega \simeq 0, k \simeq p_{FN})(m_\pi^2 + p_{FN}^2)^2}{\tilde{\omega}^4(p_{FN})}, \quad (11)$$

and for  $\varrho = \varrho_0$  we have  $R \lesssim 1$ , whereas for  $\varrho = 2\varrho_0$  we already get  $R \sim 10$ .

As follows from numerical estimates of different  $\gamma$  factors entering (4) and (7), the main contribution to  $NN$  interaction for  $\varrho > \varrho_0$  is given by MOPE

$$\mathbf{I} \simeq \mathbf{II} \quad (12)$$


whether this channel ( $\mathcal{T} \propto (\boldsymbol{\sigma}_1 \cdot \mathbf{k})(\boldsymbol{\sigma}_2 \cdot \mathbf{k})$ ) of the reaction is not forbidden or suppressed by some specific reasons like symmetry, small momentum transfer, etc.

The  $\varrho$  meson contribution to  $NN$  interaction is partially included in  $g_{\alpha\beta}$ , other part contributing to  $\mathcal{T}$  and  $\tilde{\mathcal{T}}$  is minor ( $\propto \tilde{\omega}^2/m_\varrho^2$ ). Indeed, using that  $(\boldsymbol{\sigma}_1 \times \mathbf{k})(\boldsymbol{\sigma}_2 \times \mathbf{k}) = k^2 \boldsymbol{\sigma}_1 \boldsymbol{\sigma}_2 - (\boldsymbol{\sigma}_1 \mathbf{k}) \cdot (\boldsymbol{\sigma}_2 \mathbf{k})$  the  $\rho$  exchange can be cast as

$$\delta\Gamma_{N_1 N_2}^R = \left(\frac{f_\rho}{m_\rho}\right)^2 \left\{ \frac{k^2(\boldsymbol{\sigma}_1 \boldsymbol{\sigma}_2)\gamma^2}{[\omega^2 - m_\rho^2 - k^2 - \Pi_\rho^R]} - \frac{(\boldsymbol{\sigma}_1 \mathbf{k})(\boldsymbol{\sigma}_2 \mathbf{k})\gamma^2}{[\omega^2 - m_\rho^2 - k^2 - \Pi_\rho^R]} \right\}. \quad (13)$$

We may omit contribution  $\text{Re}\Pi_\rho^R$  in the Green function since  $\text{Re}\Pi_\rho^R \ll m_\rho^2$  for  $\rho \sim m_\pi^2$  under consideration;  $\gamma$  factor is the same as for the corresponding pion (charged or neutral). First term is supposed to be included in phenomenological value of the corresponding Landau–Migdal parameter leading to its momentum dependence. Due to that the value  $g'$  gets a 30% decrease (rather than an increase discussed in some works) with the momentum at  $k = p_{FN}$  compared to the corresponding value at  $k = 0$ , see [65]. Thus one can think that  $g'(0) > g'(p_{FN})$ . Second term can be dropped as small ( $\lesssim 1/30$  of MOPE contribution at  $\rho = \rho_0$ ).

Another worry [66,67] was expressed in connection with quasielastic polarization transfer experiment at LAMPF, EMC experiment and the Drell-Yan experiment at Fermi Lab which did not observe an expected in several works a pronounced pion excess in nuclei. First optimistic estimates demonstrated the pion excess to be at (15-30)% level that was ruled out by different models which analyzed mentioned experimental results including artificially enhanced pion contribution and suppressing other important contributions. However it may well be that only in a very narrow vicinity of  $\varrho_{c\pi}$  (far beyond  $\varrho_0$ ) pion fluctuations grow at  $T = 0$  and only at  $T \neq 0$  pion excess must essentially grow in substantially wider density interval [63,64].

Let us show that some effect should be although it may be numerically rather small. Let estimate a contribution of the virtual pion sea (region of small energies  $\omega < kv_F$ ) to the sum rule. It is given by

$$S(kv_F) = \int_0^{kv_F} 2\omega A_\pi \frac{d\omega}{2\pi} = \frac{2}{\pi\beta} \left[ kv_F - \frac{\tilde{\omega}^2(k)}{\beta} \arctan \left( \frac{\beta kv_F}{\tilde{\omega}^2(k)} \right) \right] \ll 1, \quad (14)$$

$A_\pi$  is the pion spectral function,  $S(\infty) = 1$ ,  $\beta = \frac{m_N^* k_{F\pi N}^2}{\pi}$ ,  $m_N^*$  is the non-relativistic effective mass given by the relation  $(d\epsilon(p)/dp)|_{p_F} = p_F/m_N^*$ . The quantity  $S(kv_F)$  having no singularity even at  $\tilde{\omega}^2(k_0) \rightarrow 0$  is, thus, rather insensitive to the pion softening effect. Therefore mentioned experimental analysis might be not as critical to the value  $\tilde{\omega}^2(k_0)$ .

The physical reason of a contribution of virtual pions at  $\omega < kv_F$  is clear. It is the well known Landau damping associated with possibility of the virtual pion decay to the nucleon particle and hole, i.e. just with the Pauli blocking. As known from  $\pi N$  scattering experiments, pions interact with nucleons. Thus must be a contribution of virtual pions to the sum-rule for pion spectral function. There is no other way out. Therefore on a question "Where virtual pions are?" we would still suggest an old fashion answer: "They are hidden inside the matter". The question which remains is only "What is the actual value of the pion excess?" To properly answer it one needs besides the pionic contribution to elaborate all relevant specific contributions related to the phenomenon analyzed in the given concrete experiment. E.g., quasielastic polarization transfer data are reasonably fitted with a slightly increased value of the Landau-Migdal parameter  $g'$  and with inclusion of  $S$  wave repulsion at small energies [16,68,69], EMC experiment is reproduced with inclusion of the soft pion mode and other relevant effects [70].

Thus instead of FOPE+ $\varrho$  exchange, as the model of  $NN$  interaction which has been used in [6] in calculation of the emissivities of the two-nucleon reactions within the "standard scenario" of NS cooling, one should use the full  $NN$  interaction given by (4) and (7) or, simplifying, approximated by its MOPE part.

### 2.3 Renormalization of the weak interaction.

The full weak coupling vertex that takes into account  $NN$  correlations is determined by (10) where now the wavy line should be replaced by the lepton pair. Thus for the vertex of our interest,  $N_1 \rightarrow N_2 l \bar{\nu}$ , we obtain [24,16]

$$V_\beta = \frac{G}{\sqrt{2}} [\tilde{\gamma}(f')l_0 - g_A \tilde{\gamma}(g')\mathbf{l}\boldsymbol{\sigma}], \quad (15)$$

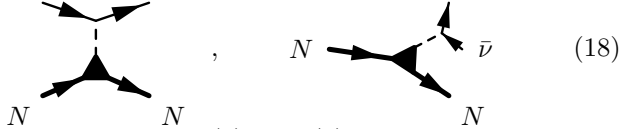
for the  $\beta$  decay and

$$V_{nn} = -\frac{G}{2\sqrt{2}} [\gamma(f_{nn})l_0 - g_A \gamma(g_{nn})\mathbf{l}\boldsymbol{\sigma}], \quad V_{pp}^N = \frac{G}{2\sqrt{2}} [\kappa_{pp}l_0 - g_A \gamma_{pp}\mathbf{l}\boldsymbol{\sigma}] \quad (16)$$

$$\kappa_{pp} = c_V - 2f_{np}\gamma(f_{nn})C_0A_{nn}, \quad \gamma_{pp} = (1 - 4gC_0A_{nn})\gamma(g_{nn}), \quad (17)$$

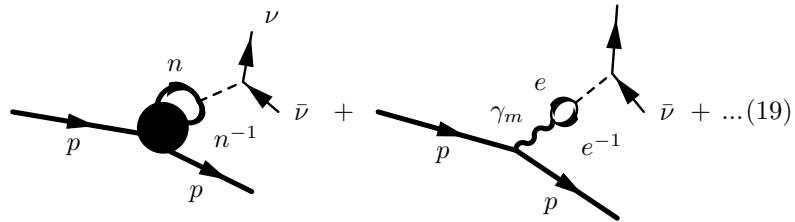
for processes on the neutral currents  $N_1 N_2 \rightarrow N_1 N_2 \nu \bar{\nu}$ ,  $V_{pp} = V_{pp}^N + V_{pp}^\gamma$ ,  $G \simeq 1.17 \cdot 10^{-5} \text{ GeV}^{-2}$  is the Fermi weak coupling constant,  $c_V = 1 - 4 \sin^2 \theta_W$ ,  $\sin^2 \theta_W \simeq 0.23$ ,  $g_A \simeq 1.26$  is the axial-vector coupling constant, and  $l_\mu = \bar{u}(q_1)\gamma_\mu(1 - \gamma_5)u(q_2)$  is the lepton current. The pion contribution  $\sim \mathbf{q}^2$  is small for typical  $|\mathbf{q}| \simeq T$  or  $p_{Fe}$ , and for simplicity is omitted. In medium the value of  $g_A$  (i.e.  $g_A^*$ ) slightly decreases with the density that can be easily incorporated, cf. the Brown–Rho scaling idea [71]. Please notice that with a decrease of  $g_A^*$ , in particular, the value  $\rho_{c\pi}$  increases remaining however to be finite ( $\simeq 2\rho_0$  according to [72] where this decrease of  $g_A^*$  up to 1 was discussed) due to attractive contribution of the  $\Delta$  isobar in (9), whereas one would expect  $\rho_{c\pi} \rightarrow \infty$  for  $g_A^* \rightarrow 1$  ignoring  $\Delta$  contribution.

The  $\gamma$  factors renormalize the corresponding vacuum vertices. These factors are essentially different for different processes involved. The matrix elements of the neutrino/antineutrino scattering processes  $N\nu \rightarrow N\nu$  and of MNB behave differently in dependence on the energy-momentum transfer and whether  $N = n$  or  $N = p$  in the  $\nu$  weak coupling vertex. Vertices



$$, \quad N \rightarrow N \bar{\nu} \quad (18)$$

are modified by the correlation factors (5) and (8). For  $N = n$  these are  $\gamma(g_{nn}, \omega, q)$  and  $\gamma(f_{nn}, \omega, q)$  leading to an enhancement of the cross sections for  $\omega > qv_{Fn}$  and to a suppression for  $\omega < qv_{Fn}$ . Renormalization of the proton vertex (vector part of  $V_{pp}^N + V_{pp}^\gamma$ ) is governed by the processes [24,73]



$$+ \dots \quad (19)$$

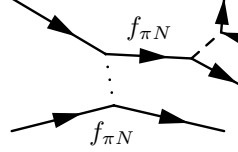
being forbidden in vacuum. For the systems with  $1S_0$  proton–proton pairing,  $\propto g_A^2$  contribution to the squared matrix element (see (16)) is compensated by the corresponding contribution of the diagram with anomalous Green functions of protons. The vector current term is  $\propto c_V^2$  in vacuum whereas it is  $\propto \kappa_{pp}^2$  in medium (by first graph (19)). Thereby the corresponding vertices with participation of proton are enhanced in medium compared to small vacuum value ( $\propto c_V^2 \simeq 0.006$ ) leading to enhancement of the cross sections, up to  $\sim 10 \div 10^2$  times for  $1.5 \div 3 \varrho_0$  depending on parameter choice. It does not contradict to the statement of ref. [24] that correlations are rather suppressed in the weak interaction vertices at  $\varrho \leq \varrho_0$ . Enhancement with the density comes from estimation (6) that directly follows from equation (2.30) of [24]. Also enhancement factor (up to  $\sim 10^2$ ) comes from the virtual in-medium photon ( $\gamma_m$ ) whose propagator contains  $1/m_\gamma^2 \sim 1/e^2$ , where  $m_\gamma$  is the effective spectrum gap, that compensates small  $e^2$  factor from electromagnetic vertices, see [73]. It is included by replacement  $V_{pp}^N \rightarrow V_{pp}$ . Other processes permitted in intermediate states like processes with  $pp^{-1}$  and with the pion are suppressed by a small proton density and by  $q^2 \sim T^2$  pre-factors, respectively. First diagram (19) was considered in [24], where the pPBF process was suggested, and then in [16,26], and it was shown that nPBF and pPBF processes may give contributions of the same order of magnitude. Finally, with electron and nucleon correlations included we recover this statement and numerical estimate [24,26] (in spite of mentioned misprints in the result [24]). Several subsequent papers [34,74,35] rediscovered pPBF process ignoring nucleon and electron correlation effects. (Although the authors were personally informed, they continue to insist [75] on incorrect treatment, giving priority to their result.) Contribution of second diagram for pPFB process was recently incorporated in [76].

Paper [27] gives another example demonstrating that, although the vacuum branching ratio of the kaon decays is  $\Gamma(K^- \rightarrow e^- + \nu_e)/\Gamma(K^- \rightarrow \mu^- + \nu_\mu) \approx 2.5 \times 10^{-5}$ , in medium (due to  $\Lambda p^{-1}$  decays of virtual  $K^-$ ) it becomes to be of order of unit. Thus we again see that in dependence of what reaction channel is considered in-medium effects may or strongly enhance the reaction rates or substantially suppress them. Ignorance of these effects may lead to misleading results where one struggling for numerical factors  $\sim 1$  may loose by orders of magnitude larger factors.

## 2.4 Inconsistencies of FOPE model

Since FOPE model became the base of the "standard scenario" for cooling simulations we would like first to demonstrate principal inconsistencies of the model for the description of interactions in dense ( $\varrho \gtrsim \varrho_0$ ) baryon medium.

The only diagram in FOPE model which contributes to the MU and NB is


(20)


Dots symbolize FOPE. This is first available Born approximation diagram, i.e. second order perturbative contribution in  $f_{\pi N}$ . In order to be theoretically consistent one should use perturbation theory up to the very same second order in  $f_{\pi N}$  for all the quantities. E.g., pion spectrum is then determined by pion polarization operator expanded up to the very same order in  $f_{\pi N}$

$$\omega^2 \simeq m_\pi^2 + k^2 + \Pi_0^R(\omega, k, \varrho), \quad \Pi_0^R(\omega, k, \varrho) = \dots \text{loop} \dots \quad (21)$$

The value  $\Pi^0(\omega, k, \varrho)$  is easily calculated containing no any uncertain parameters. For  $\omega \rightarrow 0$ ,  $k \simeq p_F$  of our interest and for isospin symmetric matter

$$\Pi_0^R \simeq -\alpha_0 - i\beta_0\omega, \quad \alpha_0 \simeq \frac{2m_N p_F k^2 f_{\pi N}^2}{\pi^2} > 0, \quad \beta_0 \simeq \frac{m_N^2 k f_{\pi N}^2}{\pi} > 0. \quad (22)$$

Replacing this value to (21) we obtain a solution with  $i\omega < 0$  already for  $\varrho > 0.3\varrho_0$  that would mean appearance of the pion condensation. Indeed, the mean field begins to increase with the time passage  $\varphi \sim \exp(-i\omega t) \sim \exp(\alpha t/\beta)$  until repulsive  $\pi\pi$  interaction will not stop its growth. But it is experimentally proven that there is no pion condensation in atomic nuclei, i.e. even at  $\varrho = \varrho_0$ . The puzzle is solved as follows. FOPE model does not work for such densities. One should replace FOPE by the full  $NN$  interaction given by (4), (7). Essential part of this interaction is due to MOPE with vertices corrected by  $NN$  correlations. Also the  $NN^{-1}$  part of the pion polarization operator is corrected by  $NN$  correlations. Thus



$$\simeq \Pi_0^R(\omega, k, \varrho) \gamma(g', \omega, k, \varrho) \quad (23)$$

being suppressed by the factor  $\gamma(g', \omega = 0, k \simeq p_F, \varrho \simeq \varrho_0) \simeq 0.35 \div 0.45$ . Final solution of the dispersion relation (21), now with full  $\Pi$  instead of  $\Pi^0$ , yields  $i\omega > 0$  for  $\varrho = \varrho_0$  whereas the solution with  $i\omega < 0$ , which shows the beginning of pion condensation, appears only for  $\varrho > \varrho_{c\pi} > \varrho_0$ .

### 3 Neutrino cooling of neutron stars

#### 3.1 Emissivity of MMU process

Since DU process is forbidden up to sufficiently high density  $\varrho_{cU}$ , the main contribution for  $\varrho < \varrho_{cU}$  and  $T_{opac} > T > T_c$  comes from MMU processes schematically presented by two diagrams of Fig. 1. MNB reactions



give smaller contribution [23]. For densities  $\rho \ll \rho_0$  the main part of the  $NN$  interaction amplitude is given by the residual  $NN$  interaction. In this case the  $NN$  interaction amplitude can be better treated within the  $T$  matrix approach which sums up the ladder diagrams in the particle-particle channel rather than by LM parameters. Calculations of MNB processes with the vacuum  $T$  matrix [77] found essentially smaller emissivity than that given by FOPE. Also the in-medium modifications of the  $T$  matrix additionally suppress the rates of both MMU and MNB processes, see [78]. Thus even at small densities the FOPE model may give only a rough estimate of the emissivity of two nucleon processes. At  $\rho \gtrsim (0.5 \div 0.7) \rho_0$  reactions in particle-hole channel and more specifically with participation of the soft pion mode begin to dominate.

Evaluations [23,42,43,16] showed that the dominating contribution to MMU rate comes from the second diagram of Fig. 1, namely from contributions to it given by the first two diagrams of the series

$$(24)$$

whereas the third diagram, which naturally generalizes the corresponding MU(FOPE) contribution, gives only a small correction for  $\rho \gtrsim \rho_0$ . The emissivity from the two first diagrams in a simplified notation [16,26] reads

$$\begin{aligned} \varepsilon^{MMU}[\text{MOPE}] &\simeq 2.4 \cdot 10^{24} T_9^8 \left(\frac{\rho}{\rho_0}\right)^{10/3} \frac{(m_n^*)^3 m_p^*}{m_N^4} \left[\frac{m_\pi}{\alpha \tilde{\omega}_{\pi^0}(p_{Fn})}\right]^4 \\ &\times \left[\frac{m_\pi}{\alpha \tilde{\omega}_{\pi^\pm}(p_{Fn})}\right]^4 \Gamma^8 F_1 \zeta(\Delta_n) \zeta(\Delta_p) \frac{\text{erg}}{\text{cm}^3 \text{sec}}, \end{aligned} \quad (25)$$

where  $T_9 = T/10^9$  K is the temperature,  $m_n^*$  and  $m_p^*$  are the nonrelativistic effective neutron and proton masses, and the correlation factor  $\Gamma^8$  is roughly

$$\begin{aligned} \Gamma^8 &\simeq \gamma_\beta^2(\omega \simeq p_{Fe}, q \simeq p_{Fe}) \gamma^2(g_{nn}, \omega \simeq 0, k = p_{Fn}) \tilde{\gamma}^4(g', 0, p_{Fn}), \\ \gamma_\beta^2(\omega, q) &= \frac{\tilde{\gamma}^2(f', \omega, q) + 3g_A^2 \tilde{\gamma}^2(g', \omega, q)}{1 + 3g_A^2}, \end{aligned} \quad (26)$$

and the second term in the factor

$$F_1 \simeq 1 + \frac{3}{4\tilde{\gamma}^2(g', 0, p_{Fn}) \gamma_\beta^2(\omega \simeq p_{Fe}, q \simeq p_{Fe})} \left(\frac{\rho}{\rho_0}\right)^{2/3} \quad (27)$$

is the contribution of the pion decay from intermediate states (first diagram (24)). The quantity  $\Gamma$  effectively accounts for an appropriate product of the

$NN$  correlation factors in different  $\pi N_1 N_2$  vertices. For charged pions the value  $\mu_\pi \neq 0$  is incorporated in the expression for the effective pion gap, for neutral pions  $\mu_\pi = 0$ . The value  $\alpha \sim 1$  depends on condensate structure,  $\alpha = 1$  for  $\varrho < \varrho_{c\pi}$ , and  $\alpha = \sqrt{2}$  taking account of the new excitations on the ground of the charged  $\pi$  condensate vacuum for  $\varrho > \varrho_{c\pi}$ . The factor

$$\zeta(\Delta_N) \simeq \begin{cases} \exp(-\Delta_N/T) & T \leq T_{cN}, \\ 1 & T > T_{cN}, \end{cases} \quad N = (n, p) \quad (28)$$

estimates the suppression caused by the  $nn$  and  $pp$  pairings. Deviation of these factors from simple exponents can be incorporated as in [35].

The ratio of the emissivities of MMU(MOPE) and MU(FOPE) is roughly

$$\frac{\varepsilon^{MMU}[\text{MOPE}]}{\varepsilon^{MU}[\text{FOPE}]} \simeq 10^3 \frac{\gamma^2(g_{nn}, 0, p_{Fn}) \tilde{\gamma}^2(g', 0, p_{Fn})}{\tilde{\omega}_{\pi^0}^4(p_{Fn}) \tilde{\omega}_{\pi^\pm}^4(p_{Fn})} (\varrho/\varrho_0)^{10/3}. \quad (29)$$

For  $\varrho \simeq \varrho_0$  this ratio is  $\sim 10$  whereas being estimated with the only third diagram (24) it would be less than unit.

### 3.2 Emissivity of DU-like processes

**NPBF processes.** The one-nucleon processes with neutral currents given by the second diagram (18) for  $N = (n, p)$  are forbidden at  $T > T_c$  by energy-momentum conservations but they can occur at  $T < T_c$ . Then physically the processes relate to NPBF, see Fig. 2. However they need special techniques to be calculated [32,24]. These processes  $n \rightarrow n\nu\bar{\nu}$  and  $p \rightarrow p\nu\bar{\nu}$  play very important role in the cooling of superfluid NS, see [24,25,16,26,36,35]. The emissivity for 3 types of neutrinos is given by [24,25]

$$\begin{aligned} \varepsilon[\text{nPBF}] &= \frac{3 \cdot 4G^2 (\xi_1 \gamma^2(f_{nn}) + \xi_2 g_A^{*2} \gamma^2(g_{nn})) p_{Fn} m_n^* \Delta_n^7}{15\pi^5} I\left(\frac{\Delta_n}{T}\right) \\ &\simeq \zeta \cdot 10^{28} \left(\frac{\varrho}{\varrho_0}\right)^{1/3} \frac{m_n^*}{m_N} \left(\frac{\Delta_n}{\text{MeV}}\right)^7 I\left(\frac{\Delta_n}{T}\right) \frac{\text{erg}}{\text{cm}^3 \cdot \text{sec}}, \quad T < T_{cn}, \end{aligned} \quad (30)$$

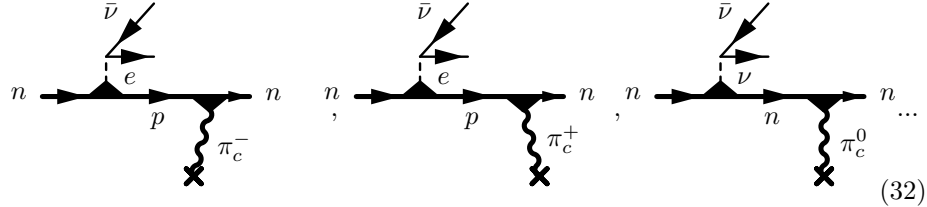
where  $\xi_1 = 1$ ,  $\xi_2 = 0$  for  $S$ -pairing and  $\xi_1 = 2/3$ ,  $\xi_2 = 4/3$  for  $P$ -pairing, compare with the result [35] where  $\xi_1 = 1$ ,  $\xi_2 = 2$  were obtained. I removed some misprints existed in [32,24,25,16]. For neutrinos  $\omega(q) = q$  and correlations are not so essential as it would be for  $\omega \ll q$ . Taking  $\gamma^2 \simeq 1.3$  in the range of  $S$ -pairing we get  $\zeta \simeq 5$  whereas for the  $P$ -pairing with  $g_A^* \simeq 1.1$  we obtain  $\zeta \simeq 9$ , in agreement with numerical evaluations [24] ( $\zeta \simeq 7$ ) used then within the cooling code in [26],  $I(x) = \int_0^\infty \text{ch}^5 y dy / (\exp(x \text{ch} y) + 1)^2$ ,  $I(x \gg 1) \simeq \exp(-2\Delta/T) \sqrt{\pi T/4\Delta}$ , that serves an appropriate asymptotic (30). Emissivity of the process  $p \rightarrow p\nu\bar{\nu}$  is given by [24]

$$\varepsilon[\text{pPBF}] = \frac{12G^2 (\xi_1 \kappa_{pp}^2 + \xi_2 g_A^{*2} \gamma_{pp}^2 + \xi_3) p_{Fp} m_p^* \Delta_p^7}{15\pi^5} I\left(\frac{\Delta_p}{T}\right), \quad T < T_{cp} \quad (31)$$

and  $\xi_2 = 0$  for protons paired in  $S$ -state in NS matter,  $\xi_3 \lesssim 1$  is due to the second diagram (19) and has a complicated structure [73,76]. For the process (31) the part of  $NN$  and  $ee$  correlations is especially important. One has  $\kappa_{pp}^2 \sim 0.05 \div 1$  for  $1 \div 3\varrho_0$  and  $\xi_3 \sim 1$ , and  $\kappa_{pp}^2 + \xi_3 \sim 1$  instead of a small  $c_V^2 \simeq 0.006$  value in absence of correlations, see discussion in subsection 2.3. Thereby, in agreement with [24,26,73,76], the emissivity of the process  $p \rightarrow p\nu\bar{\nu}$  can be compatible with that for  $n \rightarrow n\nu\bar{\nu}$  in dependence on the relation between  $\Delta_p$  and  $\Delta_n$ .

NPBF processes are very efficient for  $T < T_c$  competing with MMU processes. The former win the content for not too massive stars. Analysis of above processes supports also our general conclusion on the crucial role of in-medium effects in the cooling scenario.

**Pion (kaon) condensate processes.** The  $P$  wave pion condensate can be of three types:  $\pi_s^+$ ,  $\pi^\pm$ , and  $\pi^0$  with different values of the critical densities  $\varrho_{c\pi} = (\varrho_{c\pi^\pm}, \varrho_{c\pi_s^+}, \varrho_{c\pi^0})$ , see [57]. Thus above the threshold density for the pion condensation of the given type, the neutrino emissivity of the MMU process (25) is to be supplemented by the corresponding PU processes



The emissivity of the charged pion condensate processes with inclusion of the  $NN$  correlation effect (in a simplified treatment) renders, see [22,16],

$$\varepsilon[\text{PU}] \simeq 7 \cdot 10^{26} \frac{p_{Fn}}{m_\pi} \frac{m_n^* m_p^*}{m_N^2} \gamma_\beta^2(p_{Fe}, p_{Fe}) \tilde{\gamma}^2(g', 0, p_{Fn}) T_9^6 \sin^2 \theta \frac{\text{erg}}{\text{cm}^3 \text{sec}} \quad (33)$$

Here  $\varrho > \varrho_{c\pi}$  and  $\sin \theta \simeq \sqrt{2|\tilde{\omega}^2|/m_\pi^2}$  for  $\theta \ll 1$ . Of the same order of magnitude are emissivities of other possible  $\pi$  condensate reactions, e.g. for  $n\pi_c^0 \rightarrow npe\bar{\nu}$  process at  $\theta \ll 1$  the numerical factor is about two times larger. Since  $\pi^\pm$  condensation probably reduces the energy gaps of the superfluid states by an order of magnitude, see [79], we may assume that superfluidity vanishes above  $\varrho_{c\pi}$ . Finally we note that though the PU processes have genuinely one-nucleon phase-space volumes, their contribution to the emissivity is suppressed relative to the DU by an additional  $\tilde{\gamma}^2(g', 0, p_{Fn})$  suppression factor due to existence of the extra  $(\pi NN)$  vertex in the former case.

Fig. 4 compares the mass dependence of the neutrino cooling rates  $L_\nu/C_V$ ,  $L_\nu$  is the neutrino luminosity,  $C_V$  is the heat capacity, for MMU(MOPE) and MU(FOPE) for non-superfluid matter. For the solid curves, the neutrino emissivity in pion-condensed matter is taken into account according to (33) and (25) with the parameter  $\alpha = \sqrt{2}$ . To be conservative we took  $\varrho_{c\pi} \simeq 3\varrho_0$ . Dashed curves correspond to the model where no pion condensation is

allowed. As one sees, the medium polarization effects included in MMU may result in three order of magnitude increase of the cooling rate for the most massive stars. Even for stars of a rather low mass the cooling rate of MMU is still several times larger than for MU because even in this case the more efficient rate is given by the reactions shown by the right diagram in Fig. 1 (first two diagrams of (24)). The cooling rates for the NS of  $M = 1.8M_\odot$  with and without pion condensate differ only moderately (by factor of 5 in this model). If we would take  $\varrho_{c\pi}$  to be smaller the ratio of emissivity PU to MMU would decrease and could even become  $\lesssim 1$  in the vicinity of  $\varrho_{c\pi}$ . Opposite, the reaction rates for the FOPE model are rather independent of the star's mass for the stars with masses below the critical value  $1.63M_\odot$ , at which transition into the pion condensed phase occurs, and then jump to the typical PU value. It is to be stressed that contrary to FOPE model, the MOPE model [23] consistently takes into account the pion softening effects for  $\varrho < \varrho_{c\pi}$  and both the pion condensation and pion softening effects on the ground of the condensate for  $\varrho > \varrho_{c\pi}$ . For  $\varrho > \varrho_{cK}$  the kaon condensate processes come into

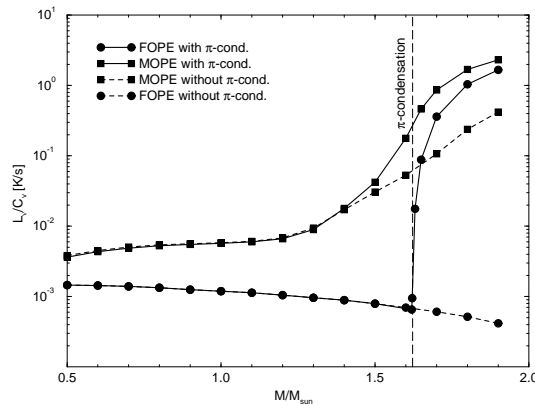


**Fig. 4.** Cooling rate due to neutrino emission as a function of star mass for a representative temperature of  $T = 3 \times 10^8$  K. Superfluidity is neglected.

play. Most popular is the idea of the  $S$  wave  $K^-$  condensation (e.g. see [13]) which is allowed at  $\mu_e > m_{K^-}^*$  due to possibility of the reaction  $e \rightarrow K^- \nu$ . Analogous condition for the pions,  $\mu_e > m_{\pi^-}^*$ , is not fulfilled owing to a strong  $S$  wave  $\pi NN$  repulsion [57,16] (again in-medium effect!) otherwise  $S$  wave  $\pi^-$  condensation would occur at smaller densities than  $K^-$  condensation. The neutrino emissivity of the  $K^-$  condensate processes is given by equation analogous to (33) with a different  $NN$  correlation factor and an additional suppression factor due to a small contribution of the Cabibbo angle. However qualitatively scenario that permits kaon condensate processes is analogous to that with the pion condensate processes.

**Other resonance processes.** There are many other reaction channels allowed in the medium. E.g, any Fermi liquid permits propagation of zero sound excitations of different symmetry related to the pion and the quanta of a more local interaction determined here via  $f_{\alpha,\beta}$  and  $g_{\alpha,\beta}$ . These excitations being present at  $T \neq 0$  may also participate in the neutrino reactions. The most essential contribution comes from the neutral current processes [23] given by first two diagrams of the series

$$\dots + \dots \quad (34)$$

Here the dotted line is zero sound quantum of appropriate symmetry. These are the resonance processes (second, of DU-type) analogous to those processes going on the condensates with the only difference that the rates of reactions with zero sounds are proportional to the thermal occupations of the corresponding spectrum branches whereas the rates of the condensate processes are proportional to the modulus squared of condensate mean field. Contribution of the resonance reactions is as a role rather small due to a small phase space volume ( $q \sim T$ ) associated with zero sounds. Please also bear in mind an analogy of the processes (34) with the corresponding phonon processes in the crust.

**DU processes.** The proper DU processes in matter, as  $n \rightarrow pe^- \bar{\nu}_e$  and  $pe^- \rightarrow n\nu_e$ ,

$$\dots \quad (35)$$

should also be treated with the full vertices. They are forbidden up to the density  $\varrho_{cU}$  when triangle inequality  $p_{Fn} < p_{Fp} + p_{Fe}$  begins to fulfill. For traditional EQS like that given by the variational theory [18] DU processes are permitted for  $\varrho > 5\varrho_0$ . The emissivity of the DU processes renders

$$\varepsilon^{DU} \simeq 1.2 \cdot 10^{27} \frac{m_n^* m_p^*}{m_N^2} \left( \frac{\mu_l}{100 \text{MeV}} \right) \gamma_\beta^2 \min[\zeta(\Delta_n), \zeta(\Delta_p)] T_9^6 \frac{\text{erg}}{\text{cm}^3 \text{sec}}, \quad (36)$$

where  $\mu_l = \mu_e = \mu_\mu$  is the chemical potential of the leptons in MeV. In addition to the usually exploited result [15], (36) contains  $\gamma_\beta^2$  pre-factor (15) due to  $NN$  correlations in the  $\beta$  decay vertices, see [24,26].

It was realized in [80] that the softening of the pion mode in dense neutron matter could also give rise to a rearrangement of single-fermion degrees of freedom due to violation of Pomeranchuk stability condition for  $\varrho = \varrho_{cF} <$

$\varrho_{c\pi}$ . It may result in organization of an extra Fermi sea for  $\varrho_{cF} < \varrho < \varrho_{c\pi}$  and at small momenta  $p < 0.2p_{Fn}$ , that in its turn opens a DU channel of neutrino cooling of NS from the corresponding layer. Due to the new feature of a temperature-dependent neutron effective mass,  $m_n^* \propto 1/T$ , we may anticipate extra essential enhancement of the DU process, corresponding to a reduction in the power of the temperature dependence from  $T^6$  to  $T^5$ . At early hot stage this layer becomes to be opaque for the neutrinos slowing the transport from the massive NS core to the exterior.

Basing on the Brown–Rho scaling idea [71], we argued in [81] for the charged  $\varrho$  meson condensation at a relevant density ( $\varrho_{c\varrho} \sim 3\varrho_0$  if  $m_\varrho^*$  would decrease to that density up to  $m_\varrho/2$ ). If happened, it would open DU reaction already for  $\varrho < \varrho_{c\varrho}$  and close it for  $\varrho > \varrho_{c\varrho}$  due to an essential modification of the nuclear asymmetry energy.

### 3.3 Comparison with soft $X$ ray data

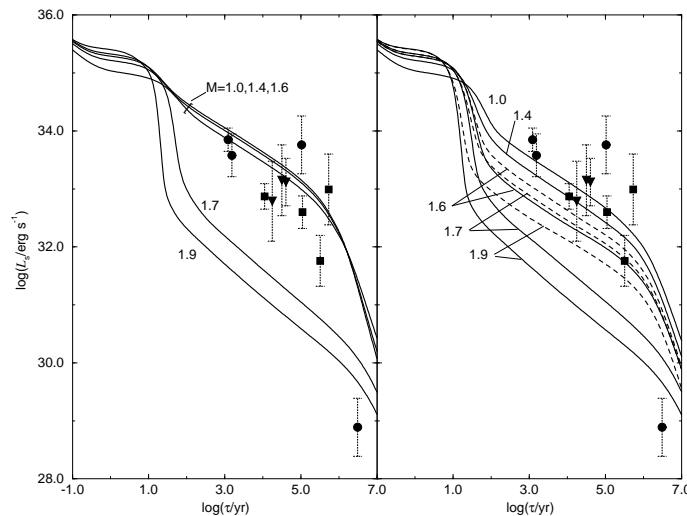


**Fig. 5.** Cooling of non-superfluid NS models of different masses constructed for the HV EOS [26]. Two graphs refer to cooling via MU(FOPE) +PU (left) and MMU(MOPE)+PU (right). In both cases, pion condensation is taken into account for the solid curves at  $\varrho > \varrho_{c\pi}$ , i.e. for  $M > 1.6M_\odot$  ( $\varrho_{c\pi}$  is chosen to be  $3\varrho_0$ ). The dashed curves in the right graph refer to a somewhat larger value of  $\tilde{\omega}^2(p_{Fn})$ , without pion condensation. The observed luminosities are labeled by dots. Possibilities of Fermi sea rearrangement and  $\varrho^\pm$  condensation are ignored.

The heat transport within the crust establishes homogeneous density profile at times  $\lesssim (1 \div 10)\text{yr}$ . After that time the subsequent cooling is determined by simple relation  $C_V \dot{T} = -L$ , where  $C_V = \sum_i C_{V,i}$  and  $L = \sum_i L_i$

are sums of the partial contributions to the heat capacity (specific heat integrated over the volume) and the luminosity (emissivity integrated over the volume).

The nucleon pairing gaps are rather purely known. Therefore one may vary them. The "standard" and "nonstandard" scenarios of the cooling of NS of several selected masses for suppressed gaps are demonstrated in the left panel of Fig. 5, [26]. Depending on the star mass, the resulting photon luminosities are basically either too high or too low compared to those given by observations. Situation changes, if the MMU process (25) is included. Now, the cooling rates vary smoothly with the star mass (see right panel of Fig. 5) such that the gap between *standard* and *non-standard* cooling scenarios is washed out. More quantitatively, by means of varying the NS mass between  $(1 \div 1.6) M_{\odot}$ , one achieves an agreement with a large number of observed data points. This is true for a wide range of choices of the  $\tilde{\omega}^2$  parameterization, independently whether pion (kaon) condensation can occur or not. Two parameterizations presented in Fig. 5 with pion condensation for  $\varrho > 3\varrho_0$  and without it differ only in the range which is covered by the cooling curves. The only point which does not agree with the cooling curves belongs to the hottest pulsar PSR 1951+32. Other three points which according to Fig. 5, right panel, are also not fitted by the curves can be easily fitted by slight changes of the model parameters. The high luminosity of PSR 1951+32 may be due to internal heating processes, cf. [10].

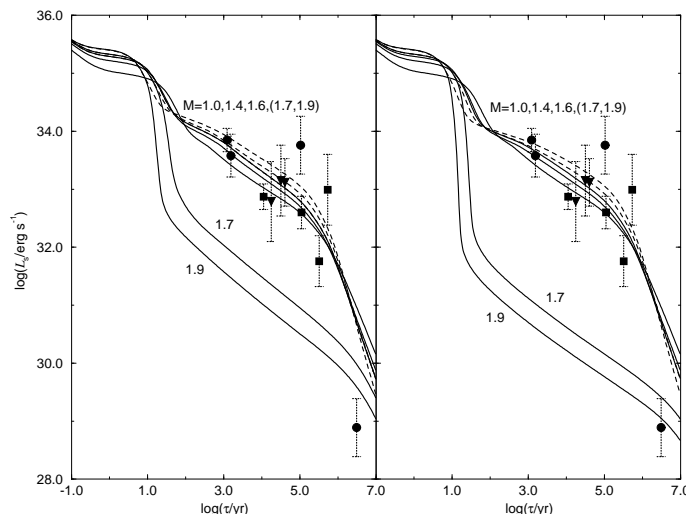


**Fig. 6.** Cooling of NS with different masses constructed for the HV EOS [26]. The cooling processes are MU-VS86, PU (only solid curves), NPNF, PPBF, and DU (only in the right graph). The dashed curves refer to the  $M = 1.7$  and  $1.9 M_{\odot}$  models without pion condensate. Possibilities of Fermi sea rearrangement and  $\varrho^{\pm}$  condensation are ignored.

We turn now to cooling simulations where the MU, NPBF, DU and PU take place simultaneously. Parameters of the pairing gaps are from Fig. 6 of [26]. Fig. 6 shows the cooling tracks of stars of different masses, computed for the HV EQS. Very efficient at  $T < T_c$  become to be NPBF processes which compete with MMU processes. The former prevail for not too massive stars in agreement with estimation [24]. The DU process is taken into account in the right graph, whereas it is neglected in the left graph. The solid curves refer again to the  $\tilde{\omega}^2$  parameterization with phase transition to pion condensate, the dashed curves to the one without phase transition (see Fig. 4). For masses in the range between 1.0 and 1.6  $M_\odot$ , the cooling curves pass through most of the data points. We again recognize a photon luminosity drop by more than two orders of magnitude for the 1.7  $M_\odot$  mass star with pion condensate, due to suppression of the pairing gaps in this case. This drop is even larger if the DU is taken into account (right graph). This allows to account for the photon luminosity of PSR 1929+10.

Thus, comparison with the observed luminosities shows that one gets quite good agreement between theory and observations if one includes into consideration all available in-medium effects assuming that the masses of the pulsars are different. We point out that the description of these effects is constructed in essentially the same manner for all the hadron systems as NS, atomic nuclei and heavy ion collisions, cf. [16,58].

### 3.4 Neutrino opacity

Important part of in-medium effects for description of neutrino transport at initial stage of NS cooling was discussed in [23,42,43,16], where correlation effects, pion softening and pion condensation, the latter for  $\rho > \rho_{c\pi}$ , were taken into account. The neutrino/antineutrino mean free paths can be evaluated from the corresponding kinetic equations via their widths  $\Gamma_{\nu(\bar{\nu})} = -2\text{Im}\Pi_{\nu(\bar{\nu})}^R$ , where  $\Pi^R$  is the retarded self-energy, or within the QPA for the nucleons they can be also estimated via the squared matrix elements of the corresponding reactions. Thereby the processes which the most efficiently contribute to the emissivity are at early times (for  $T \gtrsim 1$  MeV) responsible for the opacity.

In the above "nuclear medium cooling scenario" at  $T > T_c$  the most essential contribution was from MMU. Taking into account of  $NN$  correlations in the strong coupling vertices of two-nucleon processes like MMU and MNB suppresses the rates, whereas the softening of the pion propagator essentially enhances them. For rather massive NS MOPE wins the competition. The mean free path of neutrino/antineutrino in MMU processes is determined from the same diagrams (24) as the emissivity. Its calculation (see (25)) with the two first diagrams yields

$$\frac{\lambda_\nu^{MMU}}{R} \simeq \frac{1.5 \cdot 10^5}{F_1(2T)^8 T_9^4} \left(\frac{\rho_0}{\rho}\right)^{10/3} \frac{m_N^4}{(m_n^*)^3 m_p^*} \left[ \frac{\alpha \tilde{\omega}_{\pi^0}(p_{Fn})}{m_\pi} \right]^4 \left[ \frac{\alpha \tilde{\omega}_{\pi^\pm}(p_{Fn})}{m_\pi} \right]^4 \quad (37)$$



From the relation  $\lambda_\nu \simeq R$  follows evaluation of  $T_{opac}$ . With the only first diagram we get a simple estimate

$$T_9^{opac} \simeq 11 \frac{\varrho_0}{\varrho} \frac{\tilde{\omega}^2(p_{Fn}^2)}{[4\gamma(g_{nn}, 0, p_{Fn})\tilde{\gamma}(g', 0, p_{Fn})]^{1/2}} \frac{m_N}{m_N^*}. \quad (38)$$

For averaged value of the density  $\varrho \simeq \varrho_0$  corresponding to a medium-heavy NS ( $< 1.4M_\odot$ ) with  $\tilde{\omega}^2(p_{Fn}) \simeq 0.8m_\pi^2$ ,  $\tilde{\gamma} \simeq \gamma \simeq (0.3 \div 0.4)$  we get  $T_{opac} \simeq (1 \div 1.5)$  MeV that is smaller then the value  $T_{opac} \simeq 2$  MeV estimated with FOPE [6]. For  $\varrho \simeq 2\varrho_0$  that corresponds to a more massive NS we evaluate  $T_{opac} \simeq (0.3 \div 0.5)$  MeV. Thus pion softening results in a substantial decrease of neutrino/antineutrino mean free paths and the value of  $T_{opac}$ .

The diffusion equation determines the characteristic time scale for the heat transport of neutrinos from the hot zone to the star surface  $t_0 \sim R^2 C_V \sigma^{-1} T^{-3} / \lambda_\nu$  ( $\sigma$  is the Stefan–Boltzmann constant), whereas it follows that  $t_0 \sim 10$  min. for  $T \simeq 10$  MeV and  $\varrho \simeq \varrho_0$ ,  $\tilde{\omega}^2 \simeq 0.8m_\pi^2$ ,  $\Gamma \simeq 0.4$ ,  $m_N^*/m_N \simeq 0.9$ , and  $t_0$  becomes as large as several hours for  $\varrho \simeq (2 \div 3)\varrho_0$ . These estimates demonstrate that more massive NS cool down more slowly at  $T > T_{opac}$  and faster at subsequent times then the less massive stars.

Due to in-medium effects neutrino scattering cross section on the neutrons shown by the first diagram (18) requires the  $NN$  correlation factor

$$\gamma_{n\nu}^2(\omega, q) = \frac{\gamma^2(f_{nn}, \omega, q) + 3g_A^2 \gamma^2(g_{nn}, \omega, q)}{1 + 3g_A^2}, \quad (39)$$

as follows from (16). This results in a suppression of the cross sections for  $\omega < qv_{Fn}$  and in an enhancement for  $\omega > qv_{Fn}$ . Neutrino scattering cross sections on the protons are modified by

$$\gamma_{p\nu}^2(\omega, q) = \frac{\kappa^2(f_{np}, f_{nn}, \omega, q) + 3g_A^2 \gamma_{pp}^2(g_{nn}, \omega, q)}{1 + 3g_A^2}, \quad (40)$$

that results in the same order of magnitude correction as given by (39).

Also there is a suppression of the  $\nu N$  scattering and MNB reaction rates for soft neutrinos ( $\omega \lesssim (3 \div 6)T$ ) due to multiple  $NN$  collisions



$$\dots \quad (41)$$

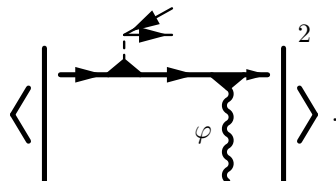
(LPM effect). One may estimate these effects simply multiplying squared matrix elements of the  $\nu N$  scattering and the MNB processes by the corresponding suppression pre-factors [28]. Qualitatively one may use a general pre-factor  $C_0(\omega) = \omega^2 / [\omega^2 + \Gamma_N^2]$ , where  $\Gamma_N$  is the nucleon width and the  $\omega$  is the energy of  $\nu$  or  $\nu\bar{\nu}$  pair. In some works, see [82,83], correction factor, like  $C_0$ , was suggested at an ansatz level. Actually one does not need any ansatz reductions. OTF, see [28], allows to calculate the rates using the exact sum

rule. The modification of the charged current processes due to LPM effect is unimportant since the corresponding value of  $\omega$  is  $\simeq p_{Fe} \gg \Gamma_N$ .

The main physical result we discussed is that in medium the reaction rates are essentially modified. A suppression arises due to  $NN$  correlations (for  $\omega \ll kv_{FN}$ ) and infra-red pre-factors (coherence effects), and an enhancement due to the pion softening (and  $NN$  correlations for  $\omega \sim q$ ) and due to opening up of new efficient reaction channels. The pion softening demonstrates that already for densities  $\varrho < \varrho_0$  the nucleon system begins to feel that it may have  $\pi$  condensate phase transition for  $\varrho > \varrho_{c\pi}$ , although this  $\varrho_{c\pi}$  value might be essentially larger than  $\varrho_0$  or even not achieved.

#### 4 The rate of radiation from dense medium. OTF

Perturbative diagrams are obviously irrelevant for calculation of in-medium processes and one should deal with dressed Green functions. The QPA for fermions is applicable if the fermion width is much less than all the typical energy scales essential in the problem ( $\Gamma_F \ll \omega_{ch}$ ). In calculation of the emissivities of  $\nu\bar{\nu}$  reactions the minimal scale is  $\omega_{ch} \simeq 6T$ , averaged  $\nu\bar{\nu}$  energy for MNB reactions. For MMU  $\omega_{ch} \simeq p_{Fe}$ . For radiation of soft quanta of fixed energy  $\omega < T$ ,  $\omega_{ch} \simeq \omega$ . Within the QPA for fermions, the reaction rate with participation of the fermion and the boson is given by [22,23]


(42)

For equilibrium ( $T \neq 0$ ) system there is the exact relation

$$\langle \hat{\varphi}_2^\dagger \hat{\varphi}_1 \rangle(p) = iD^{-+} + |\varphi_c|^2 = \frac{A_B}{\exp(\frac{\omega}{T}) - 1} + |\varphi_c|^2, \quad A_B = -2\text{Im}D^R, \quad (43)$$

where  $\langle \hat{\varphi}_2^\dagger \hat{\varphi}_1 \rangle(p)$  means the Fourier component of the corresponding non-equilibrium Green function and  $\varphi_c$  is the mean field. Thus the rate of the reaction is related to the boson spectral function  $A_B$  and the width ( $\Gamma_B$ ) being determined by the corresponding Dyson equation, see (9).  $A_B$  is the delta-function at the spectrum branches related to resonance processes, like zero sound. The poles associated with the upper branches do not contribute at small temperatures due to a tiny thermal population of those branches. There is also a contribution to  $\text{Im}D^R$  proportional to  $\text{Im}I^R$  given by the particle-hole diagram. Within the QPA taking Im part means the cut of the diagram. Thus we show [23] that this contribution is the same as that could be calculated with the help of the squared matrix element of the two-nucleon

process

(44)

This is precisely what one could expect using optical theorem. Thus unlimited series of all possible diagrams with in-medium Green functions (see (18), (32), (34), (35)) together with two-fermion diagrams (as given by (24)) and multiple-fermion diagrams (like (41)) would lead us to a double counting. The reason is that permitting the boson width effects (and beyond the QPA for fermions also permitting finite fermion widths) the difference between one-fermion, two-fermion and multiple-fermion processes in medium is smeared out. All the states are allowed and participate in production and absorption processes. Staying with the QP picture for fermions, the easiest way to avoid mentioned double counting is to calculate the reaction rates according to (42), i.e. with the help of the diagrams of the DU-like type, which already include all the contributions of the two-nucleon origin. Multiple  $NN$  collision processes should be added separately. On the other hand, it is rather inconvenient to explicitly treat all one-nucleon processes dealing with different specific quanta instead of using of the full  $NN$  interaction amplitude whenever it is possible. Besides, as we have mentioned, consideration of open fermion legs is only possible within the QPA for fermions since Feynman technique is not applicable if Green functions of ingoing and outgoing fermions have widths (that in another language means possibility of additional processes). Thus the idea came [24,28] to integrate over all in-medium states allowing all possible processes instead of specifying different special reaction channels.

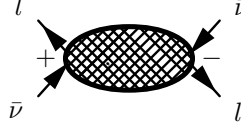
In [24,28,27] it was shown that OTF in terms of full non-equilibrium Green functions is an efficient tool to calculate the reaction rates including finite particle widths and other in-medium effects. Applying this approach, e.g., to the antineutrino-lepton (electron,  $\mu^-$  meson, or neutrino) production [24] we can express the transition probability in a direct reaction in terms of the evolution operator  $S$ ,

$$\frac{d\mathcal{W}_{X \rightarrow \bar{\nu}l}^{\text{tot}}}{dt} = \frac{(1 - n_l) dq_l^3 dq_{\bar{\nu}}^3}{(2\pi)^6 4 \omega_l \omega_{\bar{\nu}}} \sum_{\{X\}} \overline{\langle 0 | S^\dagger | \bar{\nu}l + X \rangle \langle \bar{\nu}l + X | S | 0 \rangle}, \quad (45)$$

where we presented explicitly the phase-space volume of  $\bar{\nu}l$  states; lepton occupations of given spin,  $n_l$ , are put zero for  $\nu$  and  $\bar{\nu}$  which are supposed to be radiated directly from the system (for  $T < T_{\text{opac}}$ ). The bar denotes statistical averaging. The summation goes over complete set of all possible intermediate states  $\{X\}$  constrained by the energy-momentum conservation. It was also supposed that electrons/muons can be treated in the QPA, i.e. with zero widths. Then there is no need (although possible) to consider them in intermediate reaction states. Making use of the smallness of the weak coupling,

we expand the evolution operator as  $S \approx 1 - i \int_{-\infty}^{+\infty} T \{V_W(x) S_{\text{nuc1}}(x)\} dx_0$ , where  $V_W$  is the Hamiltonian of the weak interaction in the interaction representation,  $S_{\text{nuc1}}$  is the part of the  $S$  matrix corresponding to the nuclear interaction, and  $T\{\dots\}$  is the chronological ordering operator. After substitution into (45) and averaging over the arbitrary non-equilibrium state of a nuclear system, there appear chronologically ordered ( $G^{--}$ ), anti-chronologically ordered ( $G^{++}$ ) and disordered ( $G^{+-}$  and  $G^{-+}$ ) exact Green functions.

In graphical form the general expression for the probability of the lepton (electron, muon, neutrino) and anti-neutrino production is as follows



representing the sum of all closed diagrams ( $-i\Pi^{+-}$ ) containing at least one ( $-+$ ) exact Green function. The latter quantity is especially important. Various contributions from  $\{X\}$  can be classified according to the number  $N$  of  $G^{-+}$  lines in the diagram

$$\frac{d\mathcal{W}_{\bar{\nu}l}^{\text{tot}}}{dt} = \frac{(1 - n_l)d^3q_{\bar{\nu}}d^3q_l^3}{(2\pi)^6 4\omega_{\bar{\nu}}\omega_l} \left( \begin{array}{c} l \quad \bar{\nu} \quad l \quad \bar{\nu} \\ + \quad \text{---} \quad + \quad \text{---} \quad + \quad \text{---} \quad + \quad \text{---} \\ \bar{\nu} \quad l \quad \bar{\nu} \quad l \quad \bar{\nu} \quad l \quad \bar{\nu} \end{array} \right) \quad (46)$$

This procedure suggested in [24] is actually very helpful especially if the QPA holds for the fermions. Then contributions of specific processes contained in a closed diagram can be made visible by cutting the diagrams over the ( $+ -$ ), ( $- +$ ) lines. In the framework of the QPA for the fermions  $G^{-+} = 2\pi i n_F \delta(\varepsilon + \mu - \varepsilon_p^0 - \text{Re}\Sigma^R(\varepsilon + \mu, \mathbf{p}))$  ( $n_F$  are fermionic occupations, for equilibrium  $n_F = 1/[\exp((\varepsilon - \mu_F)/T) + 1]$ ), and the cut eliminating the energy integral thus requires clear physical meaning. This way one establishes the correspondence between closed diagrams and usual Feynman amplitudes although in general case of finite fermion width the cut has only a symbolic meaning. Next advantage is that in the QPA any extra  $G^{-+}$ , since it is proportional to  $n_F$ , brings a small  $(T/\varepsilon_F)^2$  factor to the emissivity of the process. Dealing with small temperatures one can restrict by the diagrams of the lowest order in  $(G^{-+}G^{+-})$ , not forbidden by energy-momentum conservations, putting  $T = 0$  in all  $G^{++}$  and  $G^{--}$  Green functions. Each diagram in (46) represents a whole class of perturbative diagrams of any order in the interaction strength and in the number of loops.

Proceeding further we may explicitly decompose the first term in (46) as

$$\begin{array}{c} l \quad \bar{\nu} \quad l \quad \bar{\nu} \\ + \quad \text{---} \quad + \quad \text{---} \\ \bar{\nu} \quad l \quad \bar{\nu} \quad l \end{array} \quad (N=1) = \begin{array}{c} l \quad \bar{\nu} \quad l \quad \bar{\nu} \\ + \quad \text{---} \quad + \quad \text{---} \\ \bar{\nu} \quad l \quad \bar{\nu} \quad l \end{array} + \begin{array}{c} l \quad \bar{\nu} \quad l \quad \bar{\nu} \\ + \quad \text{---} \quad + \quad \text{---} \\ \bar{\nu} \quad l \quad \bar{\nu} \quad l \end{array} \quad (47)$$

The full vertex in the diagram (47) of given sign is irreducible with respect to

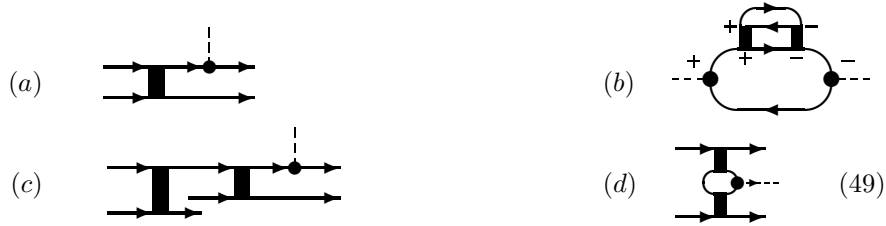
the  $(+-)$  and  $(-+)$  nucleon–nucleon hole lines. This means it contains only the lines of given sign, all  $(--)$  or  $(++)$ . Second diagram with anomalous Green functions exists only for systems with pairing. In the framework of the QPA namely these diagrams determine the proper DU and also NPBF processes calculated in [24,25] within OTF. In the QP picture the contribution to DU process vanishes for  $\rho < \rho_{cU}$ . Then the second term (46) comes into play which within the same QP picture contains two-nucleon processes with one  $(G^{-+}G^{+-})$  loop in intermediate states, etc.

The full set of diagrams for  $\Pi^{-+}$  can be further explicitly decomposed as series [28] (from now in brief notations)

$$\begin{aligned}
 -i\Pi^{-+} &= \text{bubble} + \text{bubble with vertical line} + \text{bubble with two vertical lines} + \dots \\
 &+ \text{bubble with two vertical lines and horizontal line} + \text{bubble with vertical line and horizontal line} + \text{bubble with two vertical lines and horizontal line} + \dots
 \end{aligned}
 \tag{48}$$

Full dot is the weak coupling vertex including all the diagrams of one sign,  $NN$  interaction block is the full block also of one sign diagrams. The lines are full Green functions with the widths. The most essential term is the one-loop diagram (see (47)), which is positive definite, and including the fermion width corresponds to the first term of the classical Langevin result, for details see [28]. Other diagrams represent interference terms due to rescatterings. In some simplified representations (e.g., as we used within Fermi liquid theory) the 4-point functions (blocks of  $NN$  interaction of given sign diagrams) behave like intermediate bosons (e.g. zero-sounds and dressed pions). In general it is not necessary to consider different quanta dealing instead with the full  $NN$  interaction (all diagrams of given sign). For particle propagation in an external field, e.g. infinitely heavy scattering centers (proper LPM effect), only the one-loop diagram remains, since one deals then with a genuine one-body problem. In the quasiclassical limit for fermions (with small occupations  $n_F$ ) all the diagrams given by first line of series (48) with arbitrary number of "–+" lines are summed up leading to the diffusion result, for details see [28]. For small momenta  $q$  this leads to a suppression factor of the form  $C = \omega^2/(\omega^2 + \Gamma_x^2)$ ,  $\Gamma_x$  incorporates rescattering processes. In general case the total radiation rate is obtained by summation of all diagrams in (48). The value  $-i\Pi^{-+}$  determines the gain term in the generalized kinetic equation for  $G^{-+}$ , see [84,85], that allows to use this method in non-equilibrium problems, like for description of neutrino transport in semi-transparent region of the neutrino-sphere of supernovae, as we may expect.

In the QP limit diagrams 1, 2, 4 and 5 of (48) correspond to the MMU and MNB processes related to a single in-medium scattering of two fermionic QP and can be symbolically expressed as Feynman amplitude (49a)



The one-loop diagram in (48) is particular, since its QP approximant in many cases vanishes as we have mentioned. However the full one-loop includes QP graphs of the type (49b), which survive to the same order in  $\Gamma_N/\omega_{ch}$  as the other diagrams (therefore in [24] where QP picture was used this diagram was considered as allowed diagram). In QP series such a term is included in second diagram of (46) although beyond the QPA it is included as the proper self-energy insertion to the one-loop result, i.e. in first term (46) [28]. In fact it is positive definite and corresponds to the absolute square of the amplitude (49a). The other diagrams 2, 4 and 5 of (48) describe the interference of amplitude (49a) either with those amplitudes where the weak coupling quantum ( $l\bar{\nu}$  pair) couples to another leg or with one of the exchange diagrams. For neutral interactions diagram (48:2) is more important than diagram 4 while this behavior reverses for charge exchange interactions (the latter is important, e.g., for gluon radiation from quarks in QCD transport due to color exchange interactions). Diagrams like 3 describe the interference terms due to further rescatterings of the source fermion with others as shown by (49c). Diagram (48:6) describes the production from intermediate states and relates to the Feynman graph (49d). For photons in the soft limit ( $\omega \ll \varepsilon_F$ ) this diagram (49d) gives a smaller contribution to the photon production rate than the diagram (49a), where the normal bremsstrahlung contribution diverges like  $1/\omega$  compared to the  $1/\varepsilon_F$ -value typical for the coupling to intermediate fermion lines. For  $\nu\bar{\nu}$  bremsstrahlung (49d) gives zero due to symmetry. However in some cases the process (49d) might be very important even in the soft limit. This is indeed the case for the MMU process considered above. Some of the diagrams which are not presented explicitly in (48) give more than two pieces, if being cut, so they never reduce to the Feynman amplitudes. However in the QPA they give zero contribution [28].

With  $\Gamma_F \sim \pi^2 T^2/\varepsilon_F$  for Fermi liquids, the criterion  $\Gamma_F \ll \omega_{ch} \sim T$  is satisfied for all thermal excitations  $\Delta\varepsilon \sim T \ll \varepsilon_F/\pi^2$ . However with the application to soft radiation this concept is no longer justified. Indeed series of QP diagrams is not convergent in the soft limit and there is no hope to ever recover a reliable result by a finite number of QP diagrams for the production of soft quanta. With *full Green functions*, however, one obtains a description that uniformly covers both the soft ( $\omega \ll \Gamma_F$ ) and the hard ( $\omega \gg \Gamma_F$ ) regimes. In the vicinity of  $\varrho_{c\pi}$  the quantity  $\Gamma_F$  being roughly estimated in [62,64] as  $\Gamma_F \propto \pi^2 \Gamma^2 T m_\pi/\tilde{\omega}$ , and coherence effects come into play.

In order to correct QP evaluations of different diagrams by the fermion width effects for soft radiating quanta one can simply multiply the QP results by different pre-factors [28]. E.g., comparing the one-loop result at non-zero  $\Gamma_F$  with the first non-zero diagram in the QPA ( $\Gamma_F = 0$  in the fermion Green functions) we get

$$\text{Diagram} = C_0(\omega) \left\{ \text{QPA Diagram} \right\}_{\text{QPA}}, \quad (50)$$

at small momentum  $q$ . For the next order diagrams we have

$$\begin{aligned} \text{Diagram} &= C_1(\omega) \left\{ \text{QPA Diagram} \right\}_{\text{QPA}}, \quad C_1(\omega) = \omega^2 \frac{\omega^2 - \Gamma_F^2}{(\omega^2 + \Gamma_F^2)^2}, \\ \text{Diagram} &= C_0(\omega) \left\{ \text{QPA Diagram} \right\}_{\text{QPA}}, \quad C_0(\omega) = \frac{\omega^2}{\omega^2 + \Gamma_F^2}. \end{aligned} \quad (51)$$

where factors  $C_0, C_1, \dots$  cure the defect of the QPA for soft  $\omega$ . The factor  $C_0$  complies with the replacement  $\omega \rightarrow \omega + i\Gamma_F$ . A similar factor is observed in the diffusion result, where however the macroscopic relaxation rate  $\Gamma_x$  enters, due to the resummation of all rescattering processes.

Finally, we demonstrated how to calculate the rates of different reactions in dense equilibrium and non-equilibrium matter and compared the results derived in closed diagram technique with those obtained in the standard technique of computing of the squared matrix elements.

## 5 Cooling of Hybrid Neutron Stars

Let us in addition review how the color superconducting quark matter, if exists in interiors of massive NS, may affect the neutrino cooling of HNS, [53]. A detailed discussion of the neutrino emissivity of quark matter without taking into account of the possibility of the color superconductivity has been given first in ref. [86]. In this work the quark direct Urca (QDU) reactions  $d \rightarrow ue\bar{\nu}$  and  $ue \rightarrow d\nu$  have been suggested as the most efficient processes. In the color superconducting matter the corresponding expression for the emissivity modifies as

$$\epsilon_\nu^{\text{QDU}} \simeq 9.4 \times 10^{26} \alpha_s (\varrho/\varrho_0) Y_e^{1/3} \zeta_{\text{QDU}} T_9^6 \text{ erg cm}^{-3} \text{ s}^{-1}, \quad (52)$$

where due to the pairing the emissivity of QDU processes is suppressed by a factor, very roughly given by  $\zeta_{\text{QDU}} \sim \exp(-\Delta_q/T)$ . At  $\varrho/\varrho_0 \simeq 2$  the strong coupling constant is  $\alpha_s \approx 1$  decreasing logarithmically at still

higher densities,  $Y_e = \rho_e/\rho$  is the electron fraction. If for somewhat larger density the electron fraction was too small ( $Y_e < Y_{ec} \simeq 10^{-8}$ ), then all the QDU processes would be completely switched off [87] and the neutrino emission would be governed by two-quark reactions like the quark modified Urca (QMU) and the quark bremsstrahlung (QB) processes  $dq \rightarrow uqe\bar{\nu}$  and  $q_1q_2 \rightarrow q_1q_2\nu\bar{\nu}$ , respectively. The emissivities of QMU and QB processes are smaller than that for QDU being suppressed by factor  $\zeta_{\text{QMU}} \sim \exp(-2\Delta_q/T)$  for  $T < T_{\text{crit},q} \simeq 0.4 \Delta_q$ . For  $T > T_{\text{crit},q}$  all the  $\zeta$  factors are equal to unity. The modification of  $T_{\text{crit},q}(\Delta_q)$  relative to the standard BCS formula is due to the formation of correlations as, e.g., instanton- anti-instanton molecules. The contribution of the reaction  $ee \rightarrow ee\nu\bar{\nu}$  to the emissivity is very small [88],  $\epsilon_\nu^{ee} \sim 10^{12} Y_e^{1/3} (\rho/\rho_0)^{1/3} T_9^8 \text{ erg cm}^{-3} \text{ s}^{-1}$ , but it can become important when quark processes are blocked out for large values of  $\Delta_q/T$  in superconducting quark matter.

For the quark specific heat [53] used expression of [86] being however suppressed by the corresponding  $\zeta$  factor due to color superfluidity. Therefore gluon-photon and electron contributions play important role.

The heat conductivity of the matter is the sum of partial contributions  $\kappa = \sum_i \kappa_i$ ,  $\kappa_i^{-1} = \sum_j \kappa_{ij}^{-1}$ , where  $i, j$  denote the components (particle species). For quark matter  $\kappa$  is the sum of the partial conductivities of the electron, quark and gluon components  $\kappa = \kappa_e + \kappa_q + \kappa_g$ , where  $\kappa_e \simeq \kappa_{ee}$  is determined by electron-electron scattering processes since in superconducting quark matter the partial contribution  $1/\kappa_{eq}$  (as well as  $1/\kappa_{qq}$ ) is additionally suppressed by a  $\zeta_{\text{QDU}}$  factor, as for the scattering on impurities in metallic superconductors. Due to very small resulting value of  $\kappa$  the typical time necessary for the heat to reach the star surface is large, delaying the cooling of HNS.

EQS used in ref. [53] included a model of the hadron matter, region of mixed phase and of pure quark matter. A hard EQS for the hadron matter was used, finite size effects were disregarded in description of the mixed phase, and the bag constant  $B$  was taken to be rather small that led to the presence of a wide region of mixed and quark phases already for the HNS of the mass  $M = 1.4 M_\odot$ . On the other hand, absence of a dense hadron region within this EQS allowed to diminish uncertainties in description of in-medium effects in hadronic matter suppressing them according to that used in the "standard scenario".

With the above inputs ref. [53] solved the evolution equation for the temperature profile. In order to demonstrate the influence of the size of the diquark and nucleon pairing gaps on the evolution of the temperature profile solutions were performed with different values of the quark and nucleon gaps. Comparison of the cooling evolution ( $\lg T_s$  vs.  $\lg t$ ) of HNS of the mass  $M = 1.4 M_\odot$  is given in Fig. 7. The curves for  $\Delta_q \gtrsim 1 \text{ MeV}$  are very close to each other demonstrating typical large gap behaviour. The behaviour of the cooling curve for  $t \leq 50 \div 100 \text{ yr}$  is in straight correspondence with



the heat transport processes. The subsequent time evolution is governed by the processes in the hadronic shell and by a delayed transport within the quark core with a dramatically suppressed neutrino emissivity from the color superconducting region. In order to demonstrate this feature a calculation was performed with the nucleon gaps ( $\Delta_i(n)$ ,  $i = n, p$ ) being artificially suppressed by a factor 0.2. Then up to  $\lg(t[\text{yr}]) \lesssim 4$  the behaviour of the cooling curve is analogous to the one would be obtained for pure hadronic matter. The curves labelled "MMU" show the cooling of hadron matter with inclusion of appropriate medium modifications in the  $NN$  interaction. These

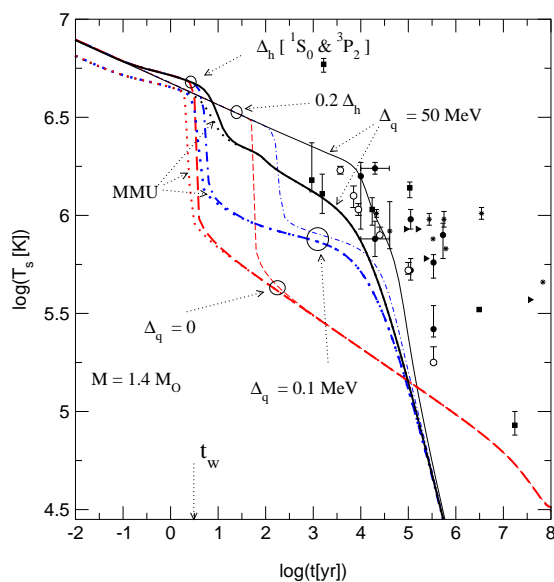


**Fig. 7.** Evolution of the surface temperature  $T_s$  of HNS with  $M = 1.4M_\odot$  for  $T_s = (10T_m)^{2/3}$ , where  $T$  is in K, see [8]. Data are from [26] (full symbols) and from [35] (empty symbols),  $t_w$  is the typical time which is necessary for the cooling wave to pass through the crust.

effects have an influence on the cooling evolution only for  $\lg(t[\text{yr}]) \lesssim 2$  since the specific model EQS used does not allow for high nucleon densities in the hadron phase at given example of HNS of  $M = 1.4 M_\odot$ . The effect would be much more pronounced for larger star masses, a softer EQS for hadron matter and smaller values of the gaps in the hadronic phase. Besides, incorporation of finite size effects within description of the mixed phase reducing its region should enlarge the size of the pure hadron phase.

The unique asymptotic behaviour at  $\lg(t[\text{yr}]) \geq 5$  for all the curves corresponding to finite values of the quark and nucleon gaps is due to a com-

petition between normal electron contribution to the specific heat and the photon emissivity from the surface since small exponentials switch off all the processes related to paired particles. This tail is very sensitive to the interpolation law  $T_s = f(T_m)$  used to simplify the consideration of the crust. The curves coincide at large times due to the uniquely chosen relation  $T_s \propto T_m^{2/3}$ .

The curves for  $\Delta_q = 0.1$  MeV demonstrate an intermediate cooling behaviour between those for  $\Delta_q = 50$  MeV and  $\Delta_q = 0$ . Heat transport becomes not efficient after first  $5 \div 10$  yr. The subsequent  $10^4$  yr evolution is governed by QDU processes and quark specific heat being only moderately suppressed by the gaps and by the rates of NPBF processes in the hadronic matter (up to  $\lg(t[\text{yr}]) \leq 2.5$ ). At  $\lg(t[\text{yr}]) \geq 4$  begins the photon cooling era.

The curves for normal quark matter ( $\Delta_q = 0$ ) are governed by the heat transport at times  $t \lesssim 5$  yr and then by QDU processes and the quark specific heat. The NPBF processes are important up to  $\lg(t[\text{yr}]) \leq 2$ , the photon era is delayed up to  $\lg(t[\text{yr}]) \geq 7$ . For times smaller than  $t_w$  (see Fig. 7) the heat transport is delayed within the crust area [15]. Since for simplicity this delay was disregarded in the heat transport treatment, for such small times the curves should be interpreted as the  $T_m(t)$  dependence scaled to guide the eye by the same law  $\propto T_m^{2/3}$ , as  $T_s$ .

For the CFL phase with large quark gap, which expected to exhibit the most prominent manifestations of color superconductivity in HNS and QCNS, [53] thus demonstrated an essential delay of the cooling during the first  $50 \div 300$  yr (the latter for QCNS) due to a dramatic suppression of the heat conductivity in the quark matter region. This delay makes the cooling of HNS and QCNS not as rapid as one could expect when ignoring the heat transport. In HNS compared to QCNS (large gaps) there is an additional delay of the subsequent cooling evolution which comes from the processes in pure hadronic matter.

In spite of that we find still too fast cooling for those objects compared to ordinary NS. Therefore, with the CFL phase of large quark gap it seems rather difficult to explain the majority of the presently known data both in the cases of the HNS and QCNS, whereas in the case of pure hadronic stars the available data are much better fitted even within the same simplified model for the hadronic matter. For 2SC (3SC) phases one may expect analogous behaviour to that demonstrated by  $\Delta_q = 0$  since QDU processes on unpaired quarks are then allowed, resulting in a fast cooling. It is however not excluded that new observations may lead to lower surface temperatures for some supernova remnants and will be better consistent with the model which also needs further improvements. On the other hand, if future observations will show very large temperatures for young compact stars they could be interpreted as a manifestation of large gap color superconductivity in the interiors of these objects.

**Concluding**, the "*nuclear medium cooling scenario*" allows easily to achieve agreement with existing data. However there remains essential uncer-

tainty in quantitative predictions due to a poor knowledge, especially, of the residual interaction treated above in an economical way within a phenomenological Fermi liquid model which needs further essential improvements. As for color superconductivity in HNS, QCNS, and QS, characterizing by large diquark pairing gaps, we did not find an appropriate fit of existing  $X$  ray data. Situation will be changed if more cold, old objects will be observed. Also, if young hot objects ( on scale  $\sim 10^2$  yr.) will be observed it could be interpreted as a signature of CFL phase in these objects.

**Acknowledgement:** Author appreciates the hospitality and support of GSI Darmstadt and ECT\* Trento. He thanks E. Kolomeitsev for discussions.

## References

1. S. Shapiro, S.A. Teukolsky: *Black Holes, White Dwarfs and Neutron Stars: The Physics of Compact Objects.* ( Wiley, New York 1983), chapter 11
2. D. Pines, R. Tamagaki, S. Tsuruta (eds.): *Neutron Stars.* (Addison-Weseley, New York 1992)
3. Ed. by M. A. Alpar, Ü. Kiziloglu, J. van Paradijs (eds.): *The Lives of the Neutron Stars* (NATO ASI Ser. C, 450; Dordrecht: Kluwer 1995)
4. J.N. Bahcall, R.A. Wolf: Phys. Rev. B **140**, 1445 (1965)
5. S. Tsuruta, A.G.W. Cameron: Canad. J. Phys. **43**, 2056 (1965)
6. B. Friman, O.V. Maxwell: Ap. J. **232**, 541 (1979)
7. O.V. Maxwell: Ap. J. **231**, 201 (1979)
8. S. Tsuruta: Phys. Rep. **56**, 237 (1979)
9. K. Nomoto, S. Tsuruta: Ap. J. Lett. **250**, 19 (1981)
10. Ch. Schaab, F.Weber, M.K. Weigel, N.K. Glendenning: Nucl. Phys. A **605**, 531 (1996)
11. G. Flowers, P.G. Sutherland, J.R. Bond: Phys. Rev. D **12**, 315 (1975)
12. O. Maxwell, G.E. Brown et al.: Ap. J. **216**, 77 (1977)
13. G.E. Brown, K. Kubodera, D. Page, P. Pizzochero: Phys. Rev. D **37**, 2042 (1988)
14. T. Tatsumi: Prog. Theor. Phys. **88**, 22 (1988)
15. J.M. Lattimer, C.J. Pethick, M. Prakash, P. Haensel: Phys. Rev. Lett. **66**, 2701 (1991)
16. A.B. Migdal, E.E. Saperstein, M.A. Troitsky, D.N. Voskresensky: Phys. Rep. **192**, 179 (1990)
17. T. Takatsuka, R. Tamagaki: Prog. Theor. Phys. **97**, 1 (1997)
18. A. Akmal, V.R. Pandharipande, D.G. Ravenhall: Phys. Rev. C **58**, 1804 (1998)
19. T. Suzuki, H. Sakai, T. Tatsumi: nucl-th/9901097
20. G.E. Brown, C.H. Lee, M. Rho, V. Thorsson: Nucl. Phys. A **567**, 937 (1994)
21. E.E. Kolomeitsev, D.N. Voskresensky, B. Kämpfer: Nucl. Phys. A **588**, 889 (1995)
22. D.N. Voskresensky, A.V. Senatorov: JETP Lett. **40**, 1212 (1984)
23. D.N. Voskresensky, A.V. Senatorov: JETP **63**, 885 (1986)
24. D.N. Voskresensky, A.V. Senatorov: Sov. J. Nucl. Phys. **45**, 411 (1987)
25. A.V. Senatorov, D.N. Voskresensky: Phys. Lett. B **184**, 119 (1987)
26. Ch. Schaab, D. Voskresensky, et al.: Astron. Astrophys. **321**, 591 (1997)

27. E.E. Kolomeitsev, D.N. Voskresensky: Phys. Rev. C **60**, 034610 (1999)
28. J. Knoll, D. N. Voskresensky: Phys. Lett. B **351**, 43 (1995); Ann. Phys. (New York) **249**, 532 (1996)
29. N.K. Glendenning: Phys. Rev. D **46**, 1274 (1992)
30. T. Tatsumi: Prog. Theor. Phys. **69**, 1137 (1983)
31. H. Umeda, K. Nomoto, et al: Ap.J. **431**, 309 (1994)
32. E. Flowers, M. Ruderman, P. Sutherland: Ap. J. **205**, 541 (1976)
33. K.P. Levenfish, D.G. Yakovlev: Astron. Reports, **38**, 247 (1994)
34. D.G. Yakovlev, A.D. Kaminker, K.P. Levenfish: Astron. Astrophys. **343**, 650 (1999)
35. D.G. Yakovlev, K.P. Levenfish, Yu.A. Shibarov: Phys. Usp. **42**, 737 (1999)
36. D. Page: *Many Faces of Neutron Stars*, ed. by R. Buccheri, J. van Paradijs, M.A. Alpar (Dordrecht, Kluwer, 1998) p. 538
37. R.F. Sawyer, A. Soni: Ap. J. **230**, 859 (1979)
38. R.F. Sawyer: Ap. J. **237**, 187 (1980)
39. R.F. Sawyer, A. Soni: Ap. J. **216**, 73 (1977)
40. S. Reddy, M. Prakash: Ap.J. **423**, 689 (1997)
41. J.A. Pons, S. Reddy, et al.: Ap.J. **513**, 780 (1999)
42. D.N. Voskresensky, A.V. Senatorov, B. Kämpfer, H. Haubold: Astrophys. Space Sci. **138**, 421 (1987)
43. H. Haubold, B. Kämpfer, A.V. Senatorov, D.N. Voskresensky: Astron. Astrophys. **191**, L22 (1988)
44. A. Sedrakian, A. Dieperink: Phys. Lett. B **463**, 145 (1999); nucl-th/0005029
45. S.Yamada: Nucl. Phys. **A662**, 219 (2000)
46. A.B. Migdal: ZhETF. **61**, 2209 (1971) (in Engl.: JETP. **34**, 1184 (1972))
47. D.N. Voskresensky, G.A. Sorokin, A.I. Chernoutsan: JETP. Lett **26**, 465 (1977)
48. N.K. Glendenning: *Compact Stars* ( New York: Springer- Verlag 1997)
49. E. Witten: Phys. Rev. D **30**, 272 (1984)
50. M. Alford, K. Rajagopal, F. Wilczek: Phys. Lett. B **422**, 247 (1998)
51. R. Rapp, T. Schäfer, E.V. Shuryak, M. Velkovsky: Phys. Rev. Lett. **81**, 53 (1998)
52. D. Blaschke, T. Klähn, D.N. Voskresensky: Ap.J. **533**, 406 (2000)
53. D. Blaschke, H. Grigorian, D.N. Voskresensky: astro-ph/0009120, Astron. Astrophys., in press (2001)
54. D. Page, M. Prakash, J.M. Lattimer, A. Steiner: Phys. Rev. Lett. **85**, 219 (2000)
55. L.D. Landau: Sov. JETP. **3**, 920 (1956)
56. A.B. Migdal: *Theory of Finite Fermi Systems and Properties of Atomic Nuclei* (Wiley and Sons, New York 1967; second. ed. (in Rus.), Nauka, Moscow, 1983)
57. A.B. Migdal: Rev. Mod. Phys. **50**, 107 (1978)
58. D. N. Voskresensky: Nucl. Phys. A **555**, 293 (1993)
59. E.E. Saperstein, S.V. Tolokonnikov: JETP Lett. **68**, 553 (1998)
60. S.A. Fayans, D. Zawischa: Phys. Lett. B **363**, 12 (1995)
61. I.N. Borzov, S.V. Tolokonnikov, S.A. Fayans: Sov. J. Nucl. Phys. **40**, 732 (1984)
62. A.M. Dyugaev: Pisma v ZhETF. **22**, 181 (1975)
63. D.N. Voskresensky, I.N. Mishustin: JETP Lett. **34**, 303 (1981); Sov. J. Nucl. Phys. **35**, 667 (1982)
64. A.M. Dyugaev: ZhETF. **83**, 1005 (1982); Sov. J. Nucl. Phys. **38**, 680 (1983)
65. A.P. Platonov, E.E. Saperstein, S.V. Tolokonnikov, S.A. Fayans: Phys. At. Nucl., **58**, 556 (1995)
66. G.F. Bertsch, L. Frankfurt and M. Strikman: Science. **259**, 773 (1993)

67. G.E. Brown, M. Buballa, Zi Bang Li and J. Wambach: Nucl. Phys. A **593**, 295 (1995)
68. M. Ericson: Nucl. Phys. A **577** (1994) 147c
69. J. Delorm, M. Ericson: Phys. Rev. C **49** (1994) 1763
70. E. Marco. E. Oset and P. Fernandez de Cordoba: Nucl. Phys. A **611**, 484 (1996)
71. G.E. Brown, M. Rho: Phys. Rev. Lett. **66**, 2720 (1991); Phys. Rep. **269**, 333 (1996)
72. G. Baym, D. Campbell, R. Dashen, J. Manassah: Phys. Lett. B **58**, 304 (1975)
73. D.N. Voskresensky, E.E. Kolomeitsev, B. Kämpfer: JETP. **87**, 211 (1998)
74. A.D. Kaminker, P. Hansel, D.G. Yakovlev: Astron. Astroph. **345**, L14 (1999)
75. D.G. Yakovlev, A.D. Kaminker, O.Y. Gnedin, P. Hansel: astro-ph/0012122
76. L.B. Leinson: Phys. Lett. B **473**, 318 (2000)
77. C. Hanhart, D. R. Phillips, and S. Reddy: nucl-th/0003445
78. D. Blaschke, G. Röpke, et al.: MNRAS. **273**, 596 (1995)
79. T. Takatsuka, R. Tamagaki: Progr. Theor. Phys. **64**, 2270 (1980)
80. D.N. Voskresensky, V. A. Khodel, M. V. Zverev, J.W. Clark: astro-ph/0003172; Ap. J. **533**, L127 (2000)
81. D.N. Voskresensky: Phys. Lett. B **392**, 262 (1997)
82. G. Raffelt, D. Seckel: Phys. Rev. D **52**, 1780 (1995)
83. S. Hannestad, G. Raffelt: astro-ph/971132
84. Yu.B. Ivanov, J. Knoll, D.N. Voskresensky: Nucl. Phys. A **672**, 314 (2000)
85. Yu.B. Ivanov, J. Knoll, H.van Hees, D.N. Voskresensky: nucl-th/0005075
86. N. Iwamoto: Ann. Phys. **141**, 1 (1982)
87. R.C. Duncan, S.L. Shapiro, I. Wasserman: ApJ **267**, 358 (1983)
88. A.D. Kaminker, P. Haensel: Acta Phys. Pol. B **30**, 1125 (1999)

